Modelling and Simulation of the Diesel Engine Injection Systems

Jiyuan Zeng

TU Delft

Modelling and Simulation of the Diesel Engine Injection Systems

By

Jiyuan Zeng

in partial fulfilment of the requirements for the degree of

Master of Science
in Maritime Technology

at the Delft University of Technology,
to be defended publicly on Monday January 29, 2019 at 14:00 PM.

Student number	4493206
Thesis number	SDPO.19.002.m.
Supervisor:	Ir. K. Visser
Thesis committee:	Ir. K. Visser
	Dr. Peter d. Vos
	Dr. Ir. G.H. Keetels
	Ir. Harsh Sapra

TU Delft

PREFACE

The three years of study in the Netherlands has been the most fascinating and challenging experience in my 24 years of life. During the three years, I feel absolutely grateful to have the chance to study in TU Delft and sip the amazing European culture.

Firstly, I would like to address my gratitude here to my supervisor Mr. Klaas Visser, who offered me a lot of help during my graduation program and always gave me the motivation to study, without him I couldn't have finished this thesis. Aside for the academic guidance, Mr. Visser also helped me a lot when it comes to the visa extension and time management. Being a student that always procrastinate, I would like to thanks to Mr. Visser again for all he did for me.

Besides, I would like to thanks to the Maritime Department of 3mE: Thanks to Mr. Loonstijn Mike for giving me an introduction on Simulink, which is very useful for me to start my project. Thanks to Mr. Harsh Sapra, who helped me very much in improving my model development, thesis writing and model verification. Every time when I asked him for help, Mr. Sapra always replied me with patience and kindness. Thanks to Mr. Peter de Vos, who helped me to pass the obligatory course in the second year of my master and handle my ECTs progress before my graduation, and I feel very grateful that Mr. de Vos will also be my graduation committee.

I also thank the external committee member, Dr. Ir. G.H. Keetels for having found time to be part of the graduation committee.

Also, I would like to thank my friends Chuan Sun and Shimeng Zhao for encouraging me and supporting me during my master, and lighting up my life when I feel very demotivated. All the journeys, band plays and hang outs have been the precious memory in my life and I would never forget.

And lastly, I would like to address my special thanks to my family. I wrote in Chinese Pinyin so my parents can read it: 'Xièxiè bàba māmā, wǒ ài nǐmen' (*thank you, Dad and Mom*).

Jiyuan Zeng
Delft, December 2018

Abstract

This thesis aims at gaining insights into the operational principles of the diesel engine injection systems and reproducing the dynamic of fuel injection in the diesel engines. Two popular fuel injection systems are modeled in this thesis.

Firstly, a cam-driven mechanical injection model is built to reproduce the operation of the mechanical injection system. The model is capable of simulating the injection rate and injection pressure by giving inputs of component geometries and the cam speed. After that, a solenoid-controlled injector model is developed to reproduce the injection process of the common rail system. For verification, the operational results of the mechanical injection system model are examined by comparing it to a real engine's injection rate provided by the Royal Dutch Navy.

CONTENTS

LIST OF FIGURES

LIST OF TABLES

1

INTRODUCTION

1.1 Research Background

Shipping is now the most popular way of global transportation due to its unique advantage of low-cost and huge capacity. One reason contributes water transportation's low cost is its application of marine diesel engines: diesel engine is the most efficient internal combustion engine in turns of thermal efficiency, and additionally, the marine diesel engines can be fueled by the low-grade heavy fuel, which is much cheaper than the distilled fuels. But now, the advantage of shipping is challenged by increasingly stringent regulations of pollution prevention. Pollution prevention and emission control have now been a popular research topic in the field of marine engineering.

For past few years, it has been a hot topic to improve combustion and emissions of compression ignition engines by optimizing the dynamic of combustion. The dynamic of combustion has a great impact on the engine's noise production, exhaust gas emission, fuel consumption, and engine efficiency. While improving the dynamic of combustion, on the other hand, is achieved by applying advanced injection systems. Modern injection systems with the electrical injectors are capable of realizing flexible injection, by which the fuel can always be injected in a correct amount and at the correct timing.

As the dynamic of combustion has been reproduced by an existing 3-zone combustion model, the fuel injection process is still not well modeled yet. In order to look into how the dynamic of fuel injection affects the behavior of a diesel engine, an injection system model is required to reproduce the dynamic of fuel injection rate and injection pressure. The thesis aims at developing injection system models which can simulate the dynamic of fuel injection.

1.2 Research Objectives

The main objective of this graduation project is to reproduce the dynamic of fuel injection in the diesel engines. Two types of injection system will be modeled in this project, which is the conventional mechanical injection system and the high-pressure common-rail injection system. These two types are chosen for the reason of popularity on the market, that the mechanical injection system is the most common injection system applied on board, and the high-pressure injection system is equipped in most of the electronically controlled diesel engines.

The main research objective is broken down into four sub-goals:

1. Literature review on the working principles and configurations of both the convention injection system and the common-rail injection system, find out the proper modeling approach.

2. Development of a conventional mechanical injection system model.

3. Development of a common-rail injection system model.

4. Verify the simulation result with the operational data from real engines.

1.3 Thesis Outline

This thesis is structured into 8 chapters.

Chapter 2 describes the working principle of the injection systems to be modeled in this project. The configuration of major components in the two injection systems are described in detail.

Chapter 3 describes the modeling approach, as well as stating the assumptions.

Chapter 4 and chapter 5 demonstrates the development of the mechanical injection model and common-rail injection model respectively.

Chapter 6 describes the verification on the simulation results, by comparing with the injection data from real engines.

Chapter 7 displays the simulation results of injection models, and additionally, the comparison of the two injection mechanisms are also included in this chapter.

Finally, in chapter 8, the conclusions of this project are drawn together with the recommendations for future work.

2

INJECTION SYSTEMS

In this chapter, the working principles of the two objective injection systems are investigated.
The injection system as a critical component of the diesel engine has been developed into many varieties. Traditionally, the fuel injection system is driven by the cam shaft; Such a system is called the ***mechanical injection system***. In this system, there's a cam-driven plunger pump pressurize fuel and supply further to the injectors, and then the injector is opened by the fuel pressure and realize the injection. Because of its reliance on the cam shaft, the mechanical injection system can only make injection at certain cam angle, precise control over the injection is difficult as well.
As a more advanced injecting technique, the ***common rail injection system*** can work out of the limitation of the cam shaft. The common rail injection system is driven by a separated electrical pump, the pump constantly works and supplies fuel at constant pressure to the common rail, an intermediate fuel reservoir. Injectors in the CR injection system is controlled by electrical valves. Such a design makes the CR injection system possible to achieve flexible injections.

2.1 Mechanical Injection System

The mechanical driving system is currently the most widely used injection system on marine diesel engines. The mechanically driven injection system has a relatively simple configuration. It can be roughly decomposed into three parts, *viz* the high-pressure plunger pump, the fuel tube, and the injector.

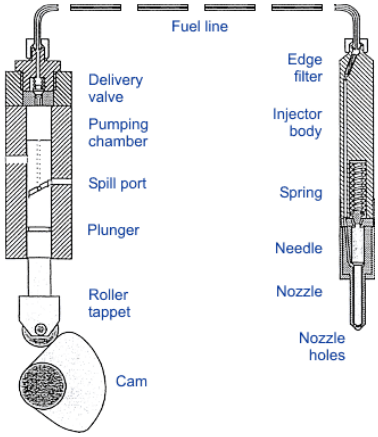

Figure 1. Mechanical injection system

The ***plunger pump***, driven by the camshaft, is responsible for receiving and pressurizing fuel, and then send the fuel to the ***injector*** via the fuel tube. The injector receives the pressurized fuel, then injects the fuel into the combustion chamber.

2.1.1 Fuel Pump

As is shown in Fig.2, the pump consists of a plunger and a barrel, which are precisely paired to ensure smooth movement and low leakage. In addition, the pump has three fuel ports: the inlet port and spill port drilled at the barrel wall and an outlet port on top. When the diesel engine is working, an auxiliary cam on the engine camshaft moves the plunger via a roller.

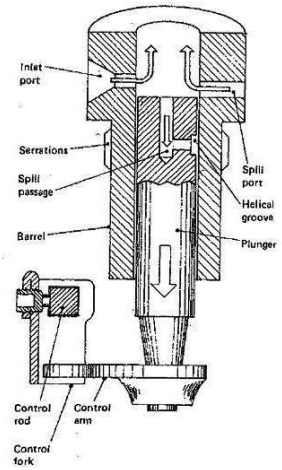

Figure 2 Scheme of the plunger pump

Fig.3 shows the operation principle of the plunger pump. During the upward stroke of the plunger, fuel is pushed out of the pump chamber through the spill port until the plunger blocks the spill port and the inlet port, subsequently the pressure inside the pump chamber quickly building up, and initiates the injection. Cams are designed in the way that fuel will be injected to the combustion chamber at a critical timing.

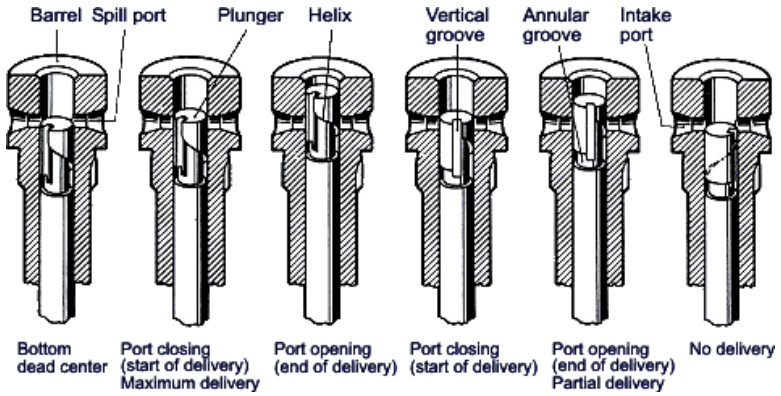

Figure 3 Operating principle of the plunger valve [1]

As the plunger continues moving up, the spill port is revealed when the lower end of plunger helical lip passes through. High pressure fuel in the pump chamber is drastically released, and fuel pressure drops down, then the fuel injection stops.

During the downward stoke, the pressure inside the pump chamber becomes low, fuel is sucked into the plunger chamber through the inlet port.

HELIX

Helix of the plunger controls the amount of supplied fuel per rotation and the timing of injection. The upper end of helix controls the starting of fuel injection as the blocking of the inlet port starts when the upper end of the helix moves higher than the inlet valve *(Fig.4B)*. The lower end of the helix controls the ending of injection, as inlet port will be open when the helix moves higher than inlet port *(Fig.4C)*. The length of the helix determines the period of port blocking, and eventually the amount of fuel being injected. The length of the helix can be adjusted by rotating the fuel rack.

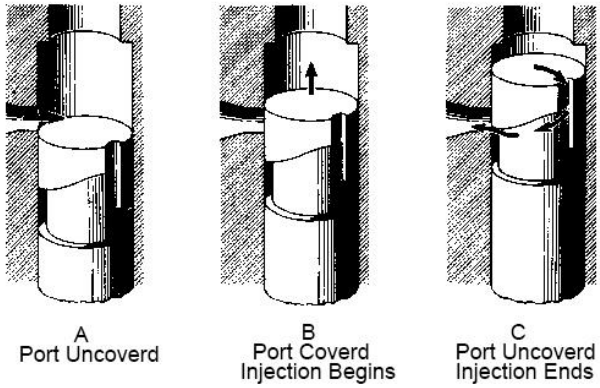

Figure 4.Function of Plunger Helix[1]

Fig 5 marks the blocking period in the plunger lift diagram to give a more intuitive view. The blocking starts once the plunger goes higher than the port ($H_p > H_{orf}$), and stops the helix passes through ($H_p < H_{orf} + L_{hlx}$).

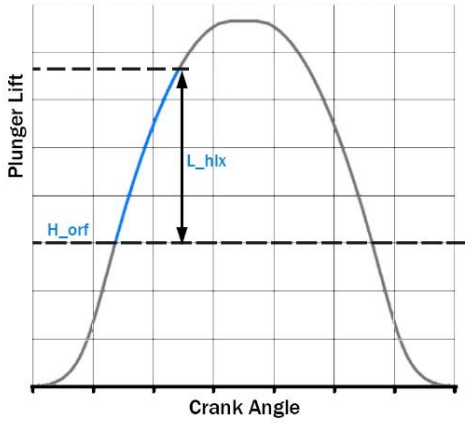

Figure 5. Period of Port Blocked

2.1.2 Mechanical Injector

There are two types of injectors in a diesel injection system. These are categorized depending upon how the fuel is injected in the system, *viz* the ***mechanical injector*** and the ***electrical injector***. The former is applied when it comes to the conventional injection systems.

The basic function of an injector is to inject fuel at a sufficient pressure. To achieve this, the mechanical injector uses the spring and needle valve to control injection pressure. The needle valve can only be lifted when fuel pressure is large enough to counter spring force. A typical structure of injector can be seen in Fig.6.

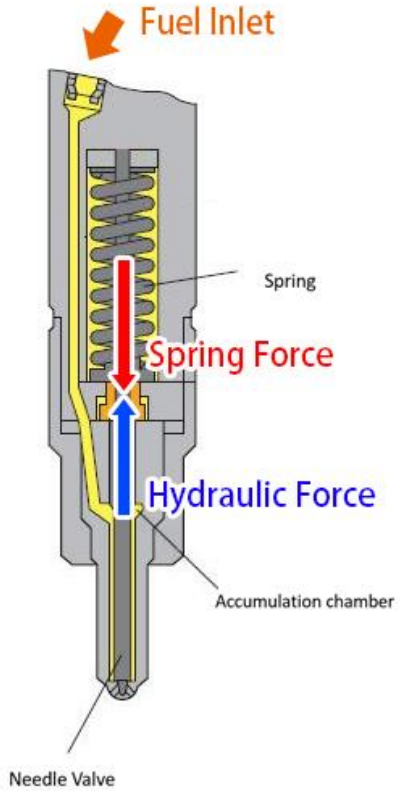

Figure 6 Mechanical Injector[2]

The fuel will firstly be trapped in the accumulation chamber when it reaches the injector. As the pressure keeps accumulating, the fuel pressure overcomes the injector's spring force and opens the valve, high-pressure fuel then, is being injected into the combustion chamber.

2.2 Common-Rail Injection System

The common rail ***(CR)*** injection system is a more advanced technique of injection. It can provide a very flexible way of injection due to the application of electrical injector, as the electrical solenoid valve can activate faster and more precise than the conventional injectors. On the other hand, the unique design of the CR system makes its fuel supply section and the fuel injection section completely independent of each other, injection becomes possible regardless of the movement of the camshaft.

In addition, with various electronic sensors, the system can monitor the engine's real-time performance parameters in all loading conditions. The parameters including RPM, cylinder pressure, temperature, fuel flow rate, etc. By sending those parameters into a microprocessor, the common rail system can adjust the injection timing, injection rate, and fuel pressure, ensuring the engine always working in the optimal condition.

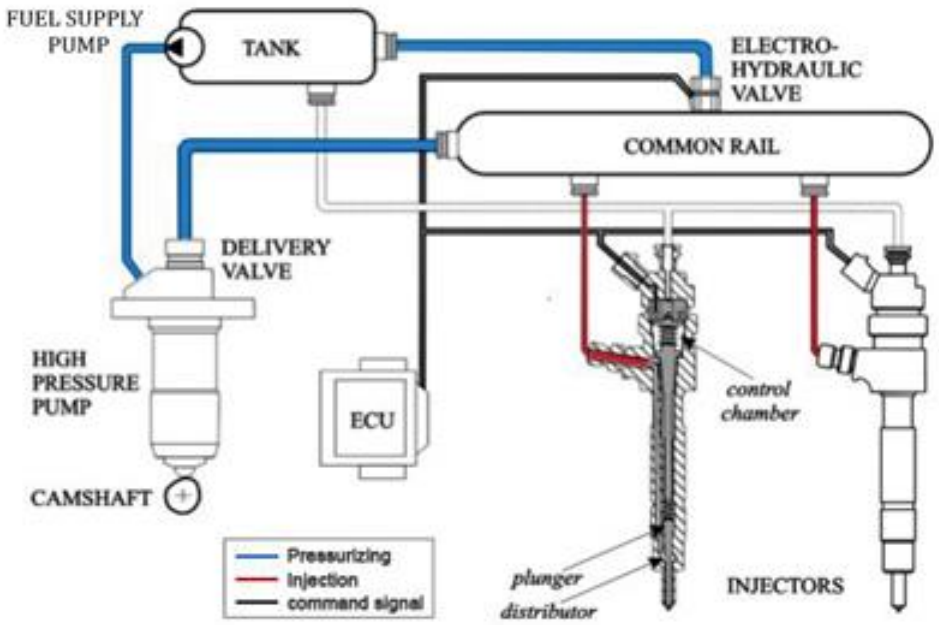

Figure 7. Scheme of Common Rail System [3]

A typical common rail system works as follows: A ***fuel supply pump*** firstly supplies fuel at low pressure to the ***high-pressure pump***, from which the fuel is pressurized. Both of the fuel supply pump and the pressurized pump are electrically driven; they constantly work to transport fuel at the designed pressure to the common rail.

The ***common rail*** is an intermediate reservoir that can collect the fuel from pumps and maintain it at a high pressure level.

Electrical-controlled ***Injectors*** in the CR system derive fuel from the rail, injecting fuel spray when they receive a command signal from the Electrical Control Unit ***(ECU)***.

The common rail injection system is able to control the fuel injection rate and realize flexible injection precisely. There are two components playing a crucial role in enabling this feature, which is the common rail and the solenoid injector.

2.2.1 Common Rail

The common rail serves as a separator between the fuel supply section and the fuel injection section. As a result, the fuel pumps can constantly work regardless of the engine's actual demand, because the common rail will always receive all the fuel they send. The injector, on the other hand, will always have enough fuel at the designed pressure whenever needed, because the rail's large capacity not only ensures sufficient fuel but also eliminates the pressure fluctuation due to intermittent pump supply and fuel injection.

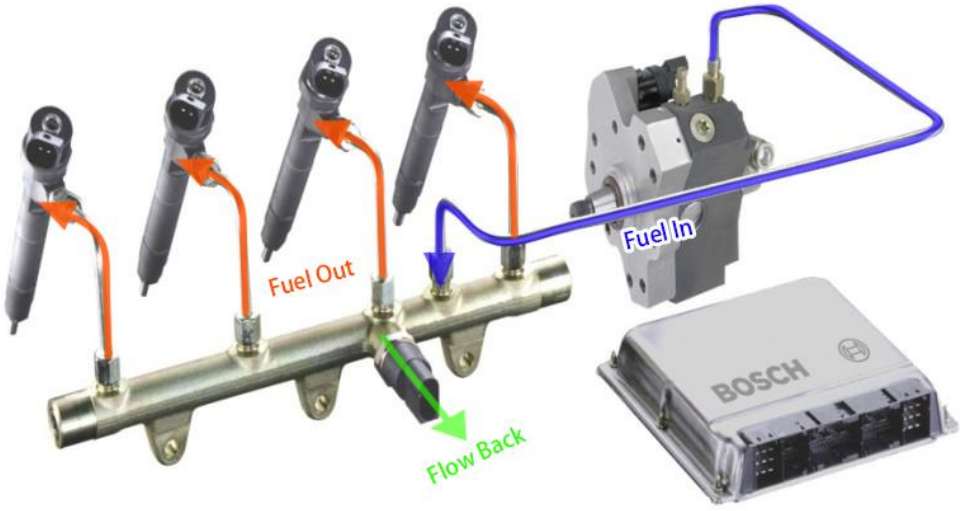

Figure 8. BOSCH Common Injection System [4]

As is illustrated in Fig. 8, the common rail has an inlet port connected to the high-pressure pump, several outlet ports connecting the injectors. Besides, the presence of a flow back tube enables the releasing of the excess fuel.

2.2.2 Electrical Injector

The injector is a complex and critical component in the injection system. It receives the high-pressure fuel from the common rail and injects the fuel through its injection holes into the combustion chamber. The injection holes are made very tiny to atomize fuel into fine droplets when the fuel is penetrating the cylinder chamber.

The solenoid nozzle can rapidly react to the command signal. Unlike the conventional injectors, the hydraulic force inside the solenoid injector is always smaller than the spring force. Its needle valve is solely controlled by the electric signal because only the combination of magnate force from the solenoid and hydraulic force can overcome the spring force. Thus, the precise control on injection, which requires the needle valve to open flexibly, becoming possible.

The working principle of electrical injectors is depicted as follows:

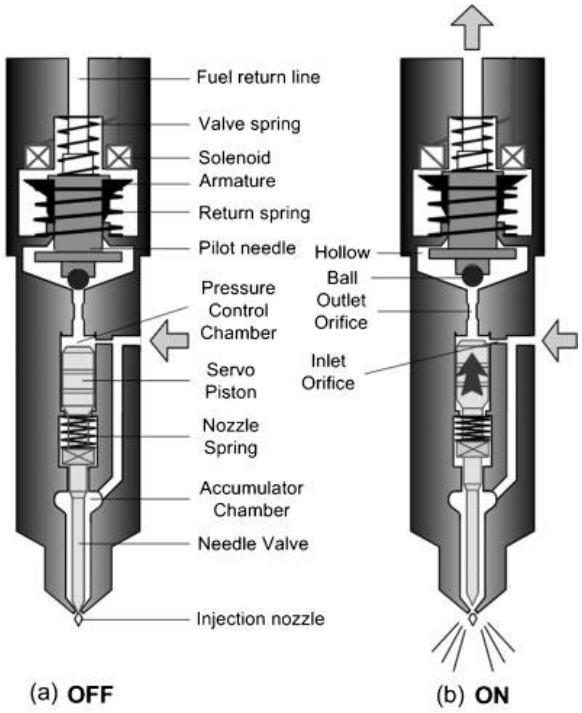

Figure 9 Electrical Injector[5]

Before the solenoid is activated, the control valve is closed, fuel enters the injector through the inlet orifice, as shown in Fig. 9(a). From which the fuel flow is divided into two paths, one part of fuel stays at the pressure control chamber which located at the upper end of the servo piston, another part of fuel goes down to the accumulation chamber, located in the middle of the needle valve. In this condition, the control chamber and the accumulator chamber were connected through orifices to the common rail. Because there was no pressure difference between the pressure control chamber and the accumulator chamber, while the area of servo piston is larger than the area of needle valve, the resultant hydraulic force is acting downward, closing the needle valve.

The injection process is depicted in Fig. 9(b). Feeding a command voltage to the solenoid for a given duration induced a magnetic force. Magnate force from the solenoid pulls the armature, together with the ball valve, upward. Subsequently, the pressure in the pressure control chamber decreased as fuel in the chamber drained into the fuel return line. In the meantime, fuel pressure in the accumulation chamber remains high, thus lifting the needle valve. Consequently, fuel starts to flow through the nozzle holes.

When the injection is over, the voltage in the solenoid together with the magnate force dissipated, the control valve closed. The fuel pressure in the pressure control chamber then increases to rail pressure again, thus the pressure difference along the needle valve together with the needle spring push the needle valve downwards, closing the valve and stop the injection process.

3

MODELLING APPROACH

3.1 Project Overview

The main objective of this thesis is to simulate the dynamic of fuel injection. To perfectly reproduce the performance of an injection system, one may need to model all the components in details and all the dynamics that the system might experience. However, such an ideal model is not practical considering the amount of information it required and its computation time. It's necessary to simplify the systems to a scale on which modeling is possible while the modeling results remain reasonable as well.

In addition, the model should be proven realistic after those simplifications. The verification work will be done upon the operation data from a test engine equipped with conventional injection system.

In conclusion, two models are required to complete the project:

- A Mechanical Injection Model
- A Common-Rail Injection Model

And each of them should be able to predict the fuel injection pressure and injection rate sufficiently accurate. A schematic summary of this graduation project is shown below:

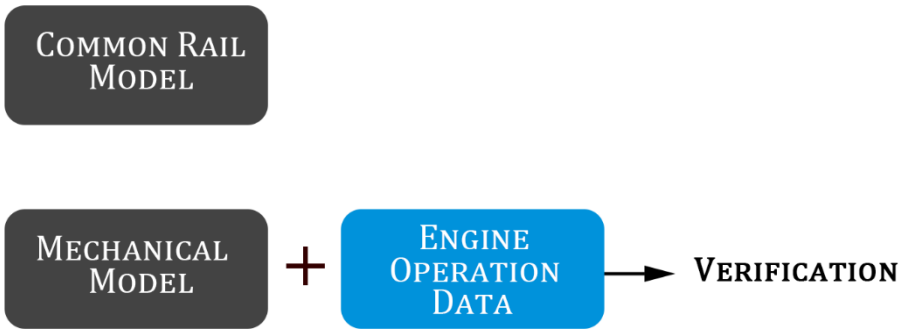

Figure 10. Project Overview

3.2 Assumptions for the Models

As a complex integration, all the components in the injection system will experience phenomena that can change their properties during the operation. The following phenomena will affect the injection result:

- Reciprocating supply and injection of fuel will induce ***pressure wave*** inside the fuel tube.**(D, T, Hountalas, et al.)** [6]
- High hydraulic pressure will induce ***deformation*** to the components and fuel tube. **(T. Sokolowski *et al.*)** [7]
- ***Cavitation*** is likely to occur inside the fuel tube and nozzle part of the injector under high injection pressure, but will not happen when the pressure is low. **(R Payri *et al.*)** [8]
- ***Eddy current*** and ***hysteresis effect*** will reduce the efficiency of the solenoid, leading to a slower respond of the actuator.

Some phenomena are negligible: The slight ***leakage*** between the matching surfaces of components causes only 10 psi pressure drop (**J. N. Anno *et al*.**) [9], and ***Pressure fluctuation*** inside the common rail various within 10 bar during operation. (**Junfeng Zhao *et al.*)** [10]

In addition, pressure and temperatures can vary in a wide range of values in a fuel injection system, which leads to a wide variety of important fuel proprieties such as ***density***, and ***kinematic viscosity***. (**Sabau *et al*.**) [11]

It's not convenient and practical to consider all the phenomena in the model, so the following assumptions are adopted to ensure the project doesn't go too far from the research scale:

- Constant fuel temperature;
- Constant fuel viscosity;
- Pressure fluctuation in common rail and fuel tube are considered zero;
- No cavitation inside the injection system;
- No leakage inside the injector;
- Laminar flow

For the electrical part, it's assumed that:

- No eddy current lost
- No hysteresis effects

For the mechanical valves, it's assumed that:

- Components are rigid;
- Collisions between the valves and the frame are consider fully inelastic, and all the kinetic energy dissipated during the collision.

3.3 Hydraulic Chambers and Mechanical Valves

Hydraulic chambers and ***mechanical valves*** are the two most common elements in the injection system.

The previous researchers modelled all the interior hollow chambers that contain fuel as the hydraulic chambers, including but not limited to the plunger chamber of the pump, the accumulation chamber, sac chamber and the pressure control chamber of the injector and the common rail. Both the flowrate between segments and the pressure in each chamber can be calculated if the hydraulic chamber model is adopted. [5], [8], [11], [12]

The mechanical valves model can reproduce the movement of the needle valve and the solenoid valve's actuator by adopting Newton's second law of motion and modifying the mass-spring-damping model. Before starting with the development, the modeling principles of these two frequent elements is investigated:

3.3.1 Hydraulic Chamber

The sketch of the hydraulic chamber model is as illustrated in Fig. 11:

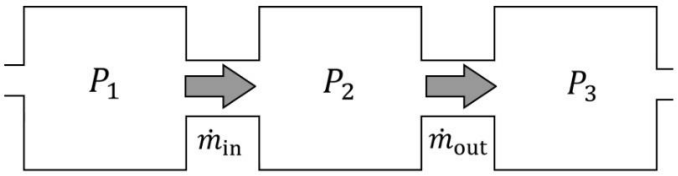

Figure 11. Hydraulic Chamber model

Liquid flows through the chambers due to pressure differences, the ***volumetric flowrate*** between the chambers can be calculated by:

$$\dot{Q} = C_d \cdot A \sqrt{\frac{2}{\rho}|P_1 - P_2|} \tag{3.1}$$

Where, $\boldsymbol{\rho}$ is the fluid density, $\boldsymbol{C_d}$ is the discharge coefficient and **A** is the cross-sectional area.

On the other hand, the pressure in the chambers changed according to the bulk modulus K_f, as the volumetric flow Q entered or left a chamber of volume V. For the diesel fuel, K_f is given by:

$$K_f = 12000(1 + 0.6\frac{P}{600}) \tag{3.2}$$

The first derivative of ***pressure*** in each chamber is given by equation (3.3):

$$\dot{P} = \frac{K_f}{V}(Q_{in} - Q_{out}) \tag{3.3}$$

Where, $\boldsymbol{Q_{in}}$ and $\boldsymbol{Q_{out}}$ are the volumetric flow rates of fuel through the inlet and outlet orifices respectively; $\boldsymbol{V}$ is the volume of chamber; $\boldsymbol{K_f}$ is the bulk modulus of fuel in the chamber.

3.3.2 Mechanical Valves

The operating principle of the needle valve and ball valve can be represented by the mass-spring-damping model:

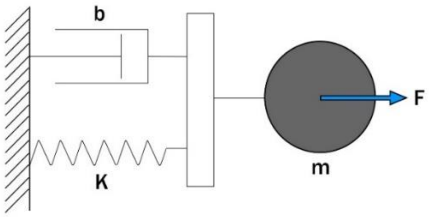

Figure 12. mass-spring-damping model

Mathematically the equation of equilibrium is represented as:

$$m\ddot{x} + b\dot{x} + kx = F(t) \tag{3.4}$$

Where, $\boldsymbol{F(t)}$ is the time dependent external force applied. For the valves, it's the hydraulic force and the magnate force; m, b and k denotes the lumped mass, damping coefficient and spring coefficient and $\boldsymbol{x, \dot{x}, \ddot{x}}$ denotes the displacement, velocity and acceleration vectors.

3.4 Discharge Coefficients and Fuel Property

Discharge coefficients and the fuel property are two types of constants widely used in this project, before the development of model, these constants are investigated to guarantee the correctness of model output.

3.4.1 Discharge Coefficients

The discharge coefficient is a dimensionless number used to characterize the flow and pressure loss behavior of nozzles and orifices in fluid systems, it's defined as the ratio between ideal flowrate and actual flow rate. Larger discharge coefficient represents lower pressure loss when passing the orifice.

According to the literature[13], the discharge coefficient for orifice are determined by the area ratio β:

$$\beta = \frac{D_0}{D_1} \tag{3.5}$$

Where, D_0 is the diameter of tube, and D_1 is the diameter of the orifice.

The area ratio of the fuel ports in the fuel pressurize pump are:

Table 1. Geometric Parameters of the Ports in the Fuel Pump

	$\boldsymbol{D_0}$ **[mm]**	$\boldsymbol{D_1}$ **[mm]**	**β**
Pump Flowback Port	125	33.94153	3.682804
Pump Delivery Port	125	24.59245	5.082861

The discharge coefficient of for orifice is calculated by[13]:

$$C_d = 1.005 - 0.471\beta + 0.564\beta^2 - 0.514\beta^3 \tag{3.6}$$

The discharge coefficient for the ports in pump are:

Table 2. Discharge Coefficient of the Ports in the Fuel Pump

	β	C_d
Pump Flowback Port	3.682804	0.850503
Pump Delivery Port	5.082861	0.896735

The discharge coefficient for the nozzles is higher compare to the orifice. Literature shows that the discharge coefficient for different types of nozzles are all higher than 0.98. In this thesis, the discharge coefficients for the injector nozzle is set as 0.98.

3.4.2 Fuel Characteristics

Some characteristics of the fuel that affects the model output are show in table below:

Table 3. Fuel Characteristics

Fuel Type	Diesel
Density	0.832 [kg/L] [14]
Bulk Modulus	$12000(1 + 0.6\frac{P}{600})$ [12]

Density of the fuel can change the flowrate under a given pressure difference, refer to equation (3.1), Larger fuel density results in larger fuel flowrate and vice versa:

$$\dot{Q} = C_d \cdot A\sqrt{\frac{2}{\rho}|P_1 - P_2|} \tag{3.1}$$

The bulk modulus of the fuel describes how resistant to compression that fuel is. It is defined as the ratio of the infinitesimal pressure increase to the resulting relative decrease of the volume.[15] The larger the bulk modulus is, the smaller volume decease under a given pressure.

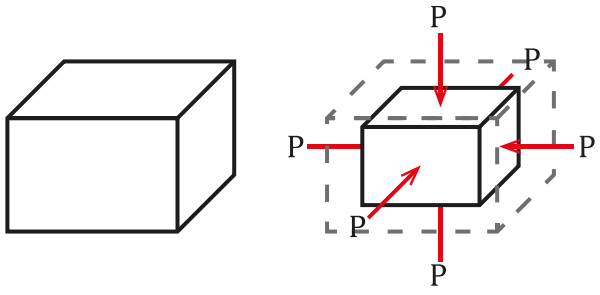

Figure 13. Illustration of Volume Change under Uniform Compression

In this project, only one type of diesel is investigated. Further research on alternative fuel is also possible by changing the fuel properties.

4

MODEL DEVELOPMENT: MECHANICAL INJECTION SYSTEM

4.1 Introduction

The mechanical injection model consists of a ***plunger pump model*** and an ***injector model***. The plunger pump is cam-driven. Thus an extra cam model is built to simulate the movement of the plunger, after which a plunger pump model computes the fuel pressure and the fuel flowrate and sends them to the injector model. The modeling high pressure pump chamber adopts the hydraulic chamber to simulate the pump pressure and outflow.

For the injector model, the movement of the needle valve is determined by the fuel pressure together with spring force. The movement of needle valve further calculates the opening of fuel nozzle area and determines the amount of injected fuel.

In conclusion of above, the following figure shows the overall structure operation sequence of the mechanical model:

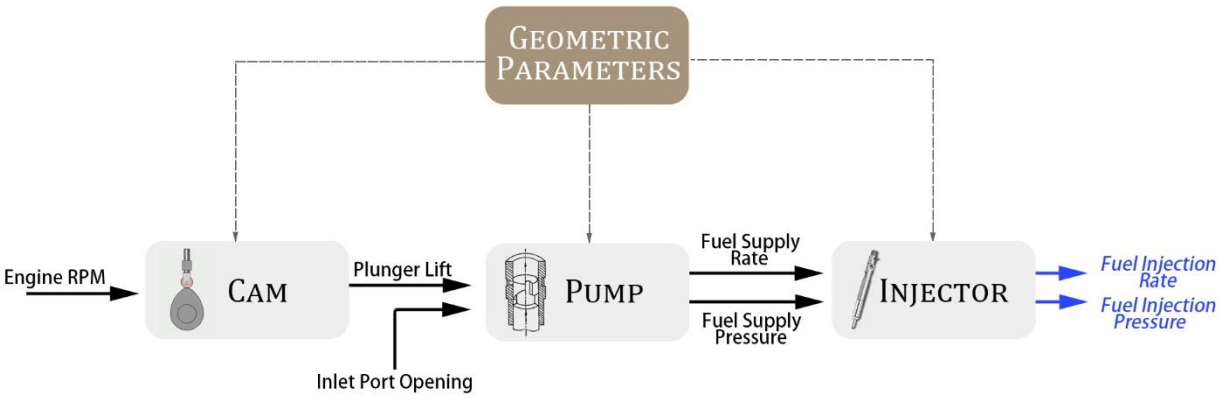

Figure 14. The configuration of the Mechanical Injection Model

The input for this model is the engine's RPM and geometric parameters of relating components, and the output is the fuel injection pressure and injection rate.

4.2 Cam

The model starts by simulating the movement of the cam shaft, which is the prime mover of the mechanical system. Fig.15 shows the scheme of a cam-follower mechanism.

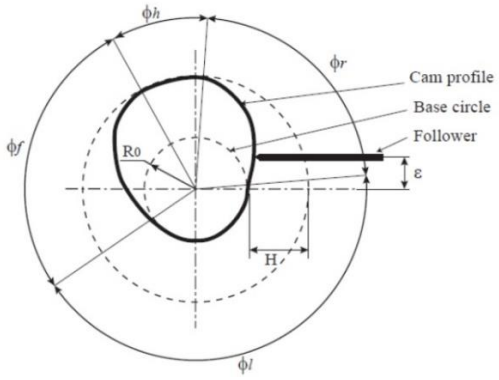

Figure 15. Cam Mechanism

Where, $\boldsymbol{\phi_r}$, $\boldsymbol{\phi_h}$, $\boldsymbol{\phi_f}$ and $\boldsymbol{\phi_l}$ denotes the rise angle, high dwell angle, fall angle and the low dwell angle,

ε denotes the eccentricity

H denotes the follower stroke.

4.2.1 Operating Principle of Cam

Displacement of the follower can be represented by a polynomial function according to (Shen Haosheng et al) [16]:

$$\mathrm{H}(\alpha) = \mathrm{H}_c(\mathrm{C}_r\beta^r + \mathrm{C}_r\beta^p + \mathrm{C}_s\beta^s + \mathrm{C}_t\beta^t) \tag{4.1}$$

In which,

$$\beta = 1 - {}^{\alpha}/_{\alpha_B} \tag{4.2}$$

Where, $\mathbf{H}(\boldsymbol{\alpha})$ is cam lift displacement; $\boldsymbol{\alpha}$ is cam angle; $\mathbf{H_c}$ is maximum lift displacement of the cam; $\boldsymbol{\alpha_B}$ is cam half wrapping angle; $\mathbf{C_r}$, $\mathbf{C_r}$, $\mathbf{C_s}$, $\mathbf{C_t}$ are underdetermined coefficients of the equation, determination of these parameters refers to literature.

Substituting the parameters from literature, the piecewise function of plunger displacement is given by equation (4.3):

$$H(\alpha) = \begin{cases} 0 & 0 < \alpha < \alpha_r \\ \mathrm{H}_c\left[35\left(\frac{\alpha}{\alpha_r}\right)^4 - 84\left(\frac{\alpha}{\alpha_r}\right)^5 + 70\left(\frac{\alpha}{\alpha_r}\right)^6 - 20\left(\frac{\alpha}{\alpha_r}\right)^7\right] & \alpha_r < \alpha < \alpha_d \\ \mathrm{H_c} & \alpha_r < \alpha < \alpha_f \\ \mathrm{H}_c\left[35\left(\frac{(\alpha_e-\alpha)}{\alpha_f}\right)^4 - 84\left(\frac{(\alpha_e-\alpha)}{\alpha_f}\right)^5 + 70\left(\frac{(\alpha_e-\alpha)}{\alpha_f}\right)^6 - 20\left(\frac{(\alpha_e-\alpha)}{\alpha_f}\right)^7\right] & \alpha_f < \alpha < \alpha_e \\ 0 & \alpha > \alpha_e \end{cases} \tag{4.3}$$

Where, $\boldsymbol{\alpha_r}$ is the angle starts rising; $\boldsymbol{\alpha_d}$ is the angle the follower reaches the maximum lift; $\boldsymbol{\alpha_f}$ is the angle starts falling; $\boldsymbol{\alpha_e}$ is the angle that the follower falls to the basic circle.

4.2.2 Cam Model

The cam model uses the pre-set engine rotating speed as the input, after which the 'current cam angle' block converts the rotation speed into the current angle of rotation.

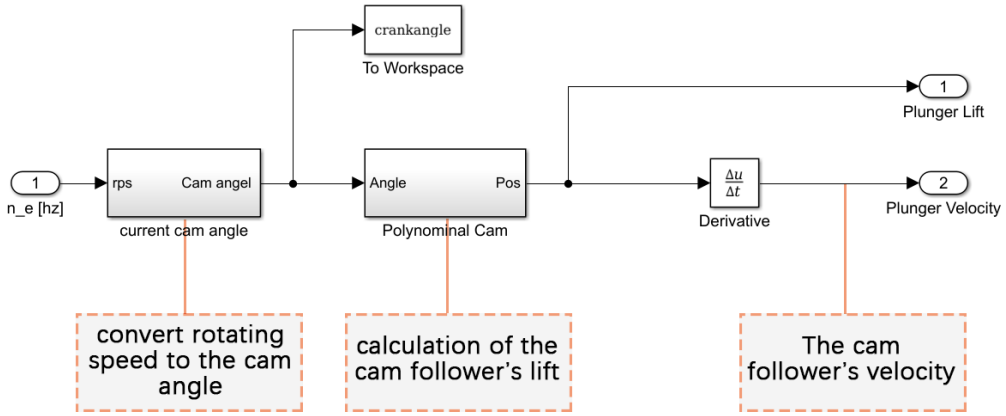

Figure 16. The Cam Model

The value of current angle subsequently enters the polynomial cam block:

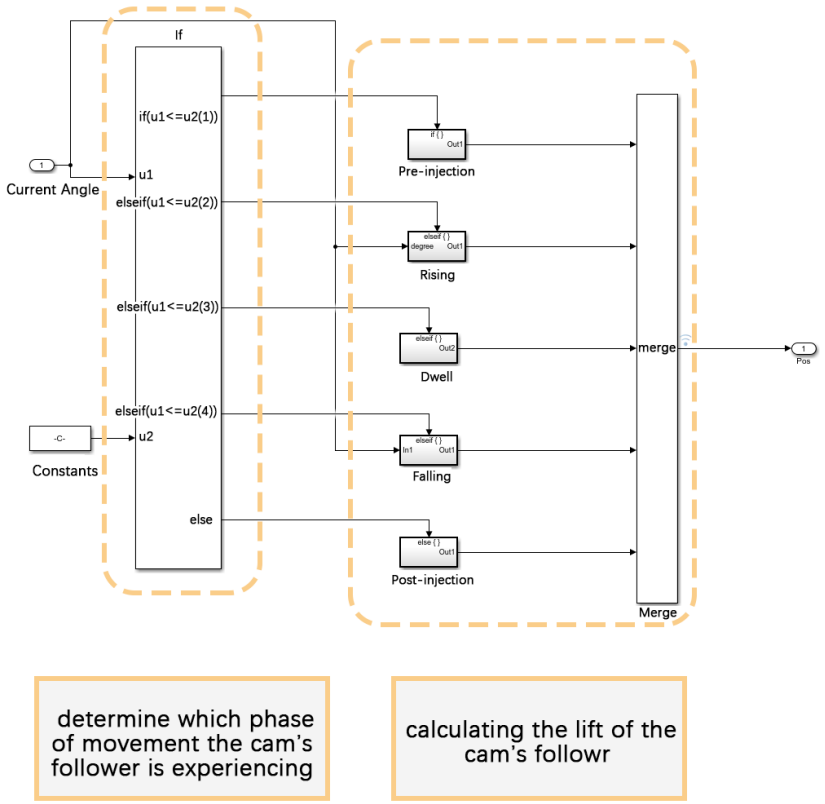

Figure 17. Polynomial Cam Block

The piecewise function of cam displacement (function (4.3)) is realized in SIMULINK using a 'If' and a 'Merge' block. In the 'If' block, the input 'u1' represents the current cam angle, and input 'u2' is the value of angle at which the cam's follower starts rising, high dwelling and falling.

The triggers in the 'If' block is activated when the cam angle is in their corresponding domains. After which a 'Merge' block is used to assemble the outputs. The output from this block is the displacement of the follower.

Table (4) shows the geometric setting of the cam model:

Table 4. Geometric setting of the cam model

$\boldsymbol{H_c}$	Follower Stroke	0.025 [m]
u2(1)	Angle of Start Rising	0°
$\boldsymbol{\phi_r}$	Rise Angle	60°
u2(2)	Angle of Start Dwelling	60°
$\boldsymbol{\phi_h}$	High Dwell Angle	0°
u2(3)	Angle of Start Falling	60°
$\boldsymbol{\phi_f}$	Fall Angle	60°
u2(4)	End of Falling	120°
$\boldsymbol{\phi_l}$	Low Dwell Angle	210°

In addition, the cam's basic circle is set as the reference surface at which the displacement of the follower is zero. It's assumed that the movement of cam's follower is identical to the movement of the plunger.

4.3 Plunger Pump

The inputs for the pump model are the ***lift*** (H_p) and ***velocity*** (v_p)of the plunger. The output from this model including the ***pressure*** inside the pump chamber and the ***flowrate*** to the injector.

The working principle of the plunger pump can be represented by the hydraulic chamber model introduced in chapter 3. One distinct feature of the plunger pump is that the volume of pump chamber is changing along with the movement of the plunger. To customize this feature, equation (3.3) is modified and put in the volume change due to plunger movement [5]:

$$\dot{P} = \frac{K_f}{V}(Q_{in} - Q_{out} + \dot{V}) \tag{4.4}$$

Where, $\boldsymbol{\dot{V}}$ is the volume change due to plunger movement, given by:

$$\dot{V} = A_p \cdot v_p \tag{4.5}$$

$\boldsymbol{V}$ is the instantaneous volume of the pump chamber:

$$V = A_p \cdot H_p \tag{4.6}$$

In the above equations, $\boldsymbol{A_p}$ is the area of plunger, $\boldsymbol{v_p}$ is the moving velocity of plunger, $\boldsymbol{H_p}$ is the lift of plunger.

Having the volume change due to plunger movement $\dot{\boldsymbol{V}}$ and the instantaneous volume $\boldsymbol{V}$, the remaining work to calculate pump pressure is to find out the volume change due to fuel flow. As shown in Fig.18, the volume change due to fuel flow $Q_{in} - Q_{out}$ consists of four parts:

$$Q_{in} - Q_{out} = q_{tank} - q_{inj} - q_{spill} - q_{leak} \tag{4.7}$$

Where, q_{tank} is the flowrate from tank to the pump chamber; q_{inj} is the flowrate supplied to the injector; q_{spill} is the flowrate of back flow fuel; q_{leak} is the flowrate that leaks.

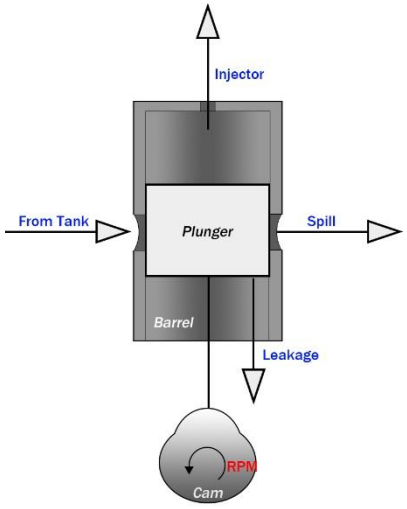

Figure 18. Fuel flows of the Pump

For the convenience of further explanation, the operation process of the fuel pump is dissected into three operational phases depending on the flow direction:

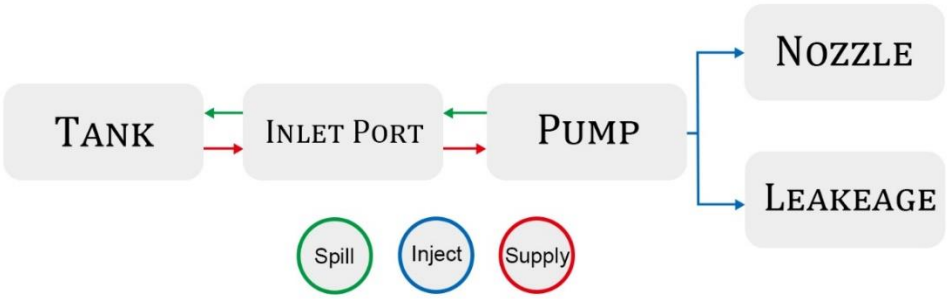

Figure 19. Three Phases of Fuel Flow

- **Spilling:** When the plunger is moving up, fuel being forced out of the pump chamber through the spill port until the injection starts; the spilling happens again right after the injection, at which the pressure in the pump chamber is much higher than the tank pressure and pushing the fuel back to the tank. The fuel flowrate in this phase is q_{spill}.
- **Injection:** During the injection fuel is forced into the injector, and a trace amount of fuel is leaked through the clearance due to the high pressure in the pump chamber. The fuel flowrate in this phase is q_{inj} and q_{leak}.
- **Supplying:** When the plunger is moving down, fuel is sucked into the pump chamber from the tank to compensate for the pressure decrease due to enlarging chamber volume. The fuel flowrate in this phase is q_{supply}.

The pump model simulates q_{supply} and q_{spill} together in the '**Barrel**' block, as the two flowrates are both between the pump chamber and the tank. And then, the flowrate to the nozzle q_{inj} and the leakage q_{leak} are separately modeled in the '**To Injector**' block and the '**Leakage**' block.

4.3.1 Barrel Block

The barrel block simulates the inlet port and the spill port of the pump, calculates the fuel flow between the high-pressure pump and the tank q_{brl}. In this model, the inlet port and the spill port are integrated.

During the supplying phase, the inlet port keeps open, fuel entering the pump chamber is considered equal to the increment of volume due to plunger movement:

$$\mathrm{q}_{brl} = \mathrm{q}_{supply} = A_p \cdot V_p \tag{4.8}$$

As a result, the fuel pressure fluctuation during the supplying phase is neglected. Because the volume change due to plunger movement are immediately filled up by the supplied fuel form tank in the model.

Flowrate during the spilling phase is calculated based on the Bernoulli equation, ref to Equation (3.1). Additionally, as the plunger is moving up, the inlet port is gradually blocked and revealed, resulting a changing sectional area. Hence, a dimensionless unit ξ is introduced to represent the opening of the inlet port:

$$\mathrm{q}_{brl} = \mathrm{q}_{spill} = \xi \cdot A_{in} \cdot C_{d\_in}\sqrt{\frac{|P_\mathrm{p} - P_t|}{\rho}} \tag{4.9}$$

$$\xi = \frac{A_{in\_ublck}}{A_{in}} \tag{4.10}$$

Where, C_{d_in} is the discharge coefficient of the inlet port, A_{in} is the sectional area of the inlet port, A_{in_ublck} is the unblocked area of the inlet port and ξ is the opening of inlet port. The calculation of the opening of inlet port ξ will be further discuss in the following section.

In conclusion of above, the flowrate function for the barrel block is:

$$\mathrm{q}_{brl} = \begin{cases} A_p \cdot v_p, & v_p < 0 \\ \xi \cdot A_{in} \cdot C_{d\_in}\sqrt{\frac{|P_\mathrm{p} - P_t|}{\rho}}, & v_p \geq 0 \end{cases} \tag{4.11}$$

Opening of the Inlet Port

As shown in Fig.20, the light blue part is the unblocked area of the inlet port A_{in_ublck}. For the convenience of model development, the process of inlet port blocking is divided into six phases: (a) pre-blocking, (b) partial blocking phase 1, (c) partial blocking phase 2, (d) fully blocking phase, (e) partial blocking phase 3, (f) partial blocking phase 4 and (g) post-blocking phase. In which phase (b) and (c) represents the covering process of the inlet port, and phase (d) and (e) represents the revealing process of the inlet port.

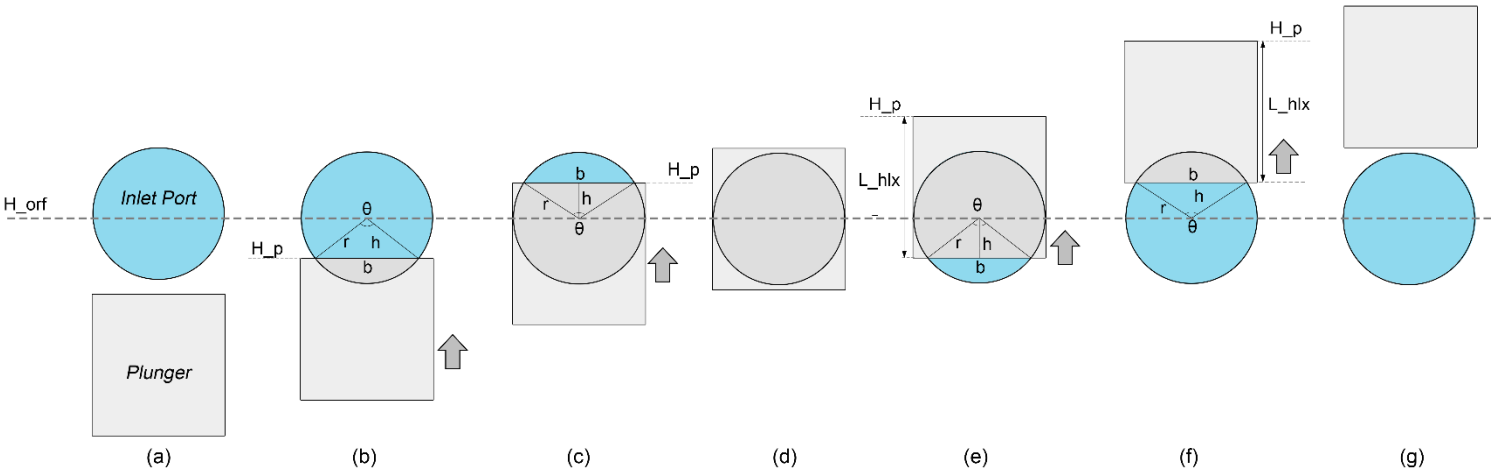

Figure 20. Blocking of the inlet port

The area of the unblocked area of the inlet port is calculated based on the lift of the plunger H_p:

- ***Partial blocking phase 1*** ($H_{orf} - r < H_p < H_{orf}$): The plunger starts covering the inlet port, but its lift is still lower than the center of the inlet port*(Fig.20b)* , the *blocked* area is given by the area of the circular sector minus the area of the triangular portion:

$$A_{blck} = A_{sector} - A_{triangle} \tag{4.12}$$

The unblocked area of the inlet port is:

$$A_{ublck} = A_{in} - A_{blck} \tag{4.13}$$

To start with the calculation, let r be the radius of the circle, b the chord length, h the height of the triangular portion.

The height h is:

$$h = H_{orf} - H_p \tag{4.14}$$

where, H_{orf} is the height of the inlet port center; H_p is the lift of the plunger.

Known the radius r, the length of the chord b is:

$$b = 2 \times \sqrt{r^2 - h^2} \tag{4.15}$$

The circular angle θ is:

$$\theta = 2 \cdot \arcsin(\frac{b/2}{r}) \tag{4.16}$$

Hence, the area of the isosceles triangle $A_{triangle}$ is:

$$A_{triangle} = \frac{1}{2} \cdot d \cdot h \tag{4.17}$$

The area of the circular sector is:

$$\mathrm{A}_{sector} = \frac{\theta}{360} \cdot A_{in} \tag{4.18}$$

Substituting in gives:

$$\mathrm{A}_{ublck} = A_{in} - (\frac{\theta}{360} \cdot A_{in} - \frac{1}{2} \cdot d \cdot h) \tag{4.19}$$

- ***Partial blocking phase 2*** ($\mathrm{H}_p > \mathrm{H}_{orf}$): The plunger moves higher than the center of the inlet port (Fig.20c), the unblocked area is directly given by the area of the circular sector minus the area of the bottom triangular portion:

$$\mathrm{A}_{ublck} = \mathrm{A}_{sector} - \mathrm{A}_{triangle} \tag{4.20}$$

Calculation of the segment area ditto this case; the only difference is the height of the triangle h:

$$\mathrm{h} = \mathrm{H}_p - \mathrm{H}_{orf} \tag{4.21}$$

- ***Total blocking phase*** ($\mathrm{H}_{orf} + r < \mathrm{H}_p < \mathrm{H}_{orf} - r + L_{hlx}$): The period when the inlet port is entirely covered by the plunger, the unblock area is zero. *(Fig.20d)*

- ***Partial blocking phase 3*** ($\mathrm{H}_{orf} - r + L_{hlx} < \mathrm{H}_p < \mathrm{H}_{orf} - L_{hlx}$): The inlet port starts revealing when the plunger helix moves higher than the inlet port *(Fig.20e)*, the revealed area is given by the area of the circular sector minus the area of the bottom triangular portion:

$$\mathrm{A}_{ublck} = \mathrm{A}_{sector} - \mathrm{A}_{triangle} \tag{4.12}$$

The height of the triangle h becomes:

$$\mathrm{h} = (\mathrm{H}_p - \mathrm{L}_{hlx}) - \mathrm{H}_{orf} \tag{4.22}$$

Ditto the remaining calculation.

- ***Partial blocking phase 4*** ($\mathrm{H}_{orf} + L_{hlx} < \mathrm{H}_p < \mathrm{H}_{orf} + r + L_{hlx}$): the plunger helix moves higher than the center of the inlet port, but not yet completely leave *(Fig.20f)*, the blocked area is given by the area of the circular sector minus the area of the bottom triangular portion:

$$\mathrm{A}_{blck} = \mathrm{A}_{sector} - \mathrm{A}_{triangle} \tag{4.23}$$

The revealed area of the inlet port is:

$$\mathrm{A}_{ublck} = A_{in} - \mathrm{A}_{blck} \tag{4.24}$$

The height of the triangle h becomes:

$$\mathrm{h} = \mathrm{H}_{orf} - (\mathrm{H}_p - \mathrm{L}_{hlx}) \tag{4.25}$$

Ditto the remaining calculation.

- ***Post-blocking phase*** and ***pre-blocking phase***($\mathrm{H}_{orf} + r < \mathrm{H}_p + L_{hlx}$ or $\mathrm{H}_{orf} - r > \mathrm{H}_p$): when the plunger completely leave the inlet port, or when the blocking process haven't started yet, the unblocked area is A_{in}:

$$\mathrm{A}_{ublck} = A_{in} \tag{4.26}$$

Fig.21 demonstrates the calculation model of the inlet port opening, which consists of four sections:

- The first section receives the ***plunger lift*** and ***plunger velocity*** as the inputs and determines the moving direction of the plunger. As the blocking of the inlet port only happens during the upward stroke of the plunger, the input signal of plunger lift is wrapped to zero when the plunger is moving downward.
- The next section receives the plunger lift signal and determines the relative position from the plunger to the inlet port, and find out the phase of blocking at the current plunger lift.
- The third section calculates the opening area of the inlet port based on the position of the plunger.
- And lastly, the unblocked area A_{ublck} is divided by the full area of the inlet port A_{in}, and outputs the dimensionless opening of the inlet port ξ.

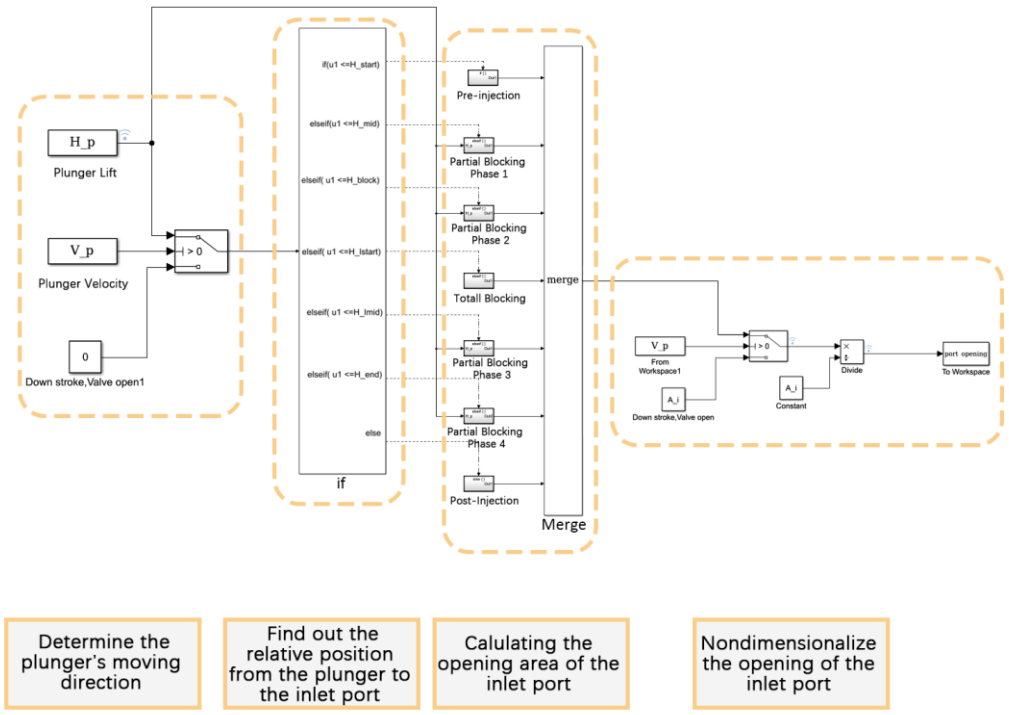

Figure 21. layout of the inlet port opening block

The constants in this model are set as follows:

Table 5. Constants in the model of inlet port opening calculation

H_start	Hight of the inlet port's lower end	$\mathbf{H_{orf} - r}$
H_mid	Hight of the inlet port's center	H_{orf}
H_block	Hight of the inlet port's upper end	$H_{orf} - r$
H_lstart	Hight of the inlet port's lower end plus the length of the plunger	$H_{orf} - r + L_{hlx}$
H_lmid	Hight of the inlet port's center plus the length of the plunger	$H_{orf} + L_{hlx}$
H_end	Hight of the inlet port's upper end plus the length of the plunger	$H_{orf} + r + L_{hlx}$
A_i	Area of the inlet port	$\pi \cdot r^2$

The operation result of the port opening model is as follows:

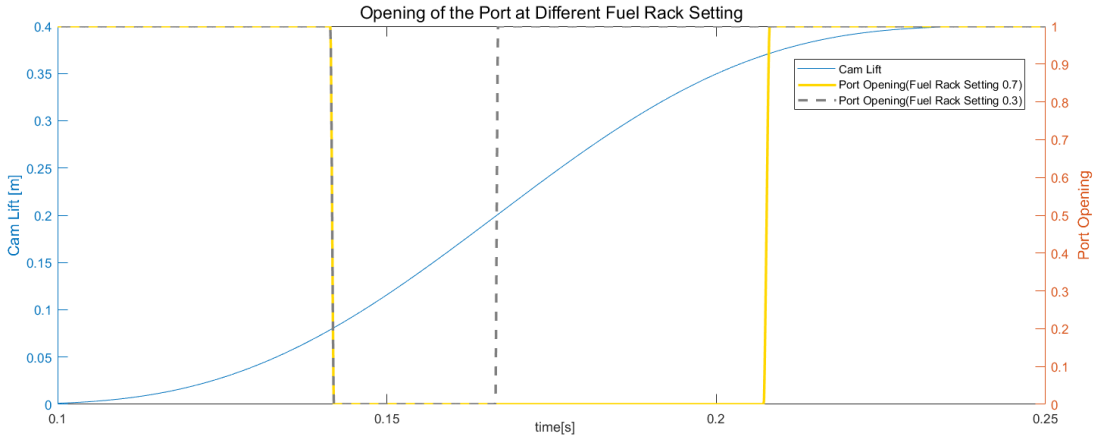

Figure 22. Port Opening at Fuel Rack Setting 0.3 and 0.7

In this model, the amount of injected fuel is adjusted by changing the blocking period of the inlet port. Figure (22) shows that the blocking period becomes longer when increase the fuel rack setting. The start of blocking, however, is determined by the height of inlet port and not affected.

Calculation of the Barrel Flowrate

The flowrate between the pump chamber and the tank is a piecewise function depends on the moving direction of the plunger:

$$q_{brl} = \begin{cases} A_p \cdot v_p, & v_p < 0 \\ \xi \cdot A_{in} \cdot C_{d_{in}} \sqrt{\frac{|P_p - P_t|}{\rho}}, & v_p \geq 0 \end{cases} \tag{4.27}$$

The sign of plunger's velocity implies the operational phase that the pump is experiencing, which the negative velocity is corresponding to the supplying phase and the positive velocity to the spilling phase. During the supplying phase, the flowrate q_{brl} is equalized to the volume change due to plunger movement $A_p \cdot v_p$, in this way the pressure fluctuation inside the pump chamber is eliminated, because the increased volume due to plunger movement is immediately filled up by fuel. The flowrate of spilling phase, on the other hand, is calculated based on the pressure difference between the pump chamber and the fuel return line. The corresponding Simulink block is built as follows: $A_{in} \cdot C_{d_{in}}$

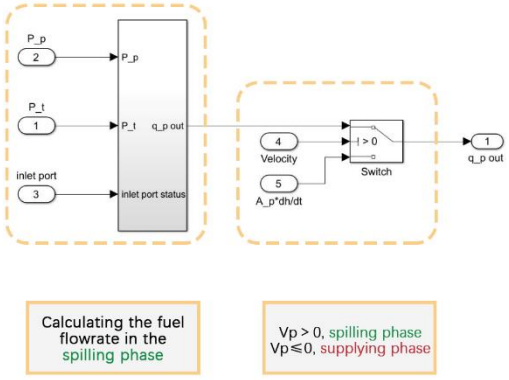

Figure 23. layout of the barrel flowrate model

Inputs for this block are the pump pressure P_p, tank pressure P_t, opening of the inlet port ξ, velocity of the plunger v_p and the volume change due to plunger movement $A_p \cdot v_p$. The output is the barrel flowrate q_{brl}, the positive direction is from the pump chamber to the tank.

The sub-block that calculating the spilling flowrate is unfold as:

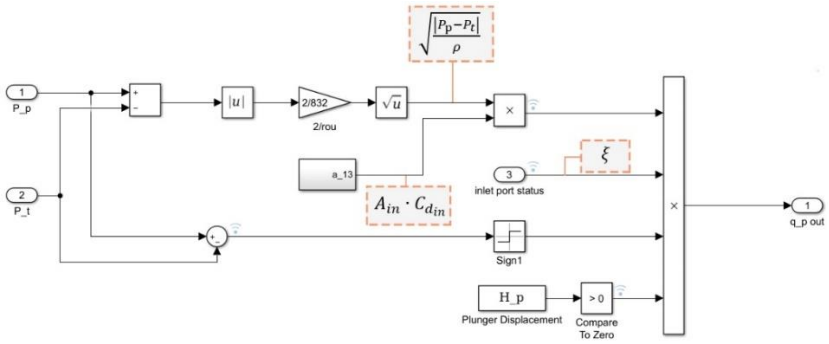

Figure 24. layout of the spilling flowrate calculation sub-block

The top two rows are doing the flowrate calculation. Besides, a 'sign' block is used to introduce the flow direction, which positive direction is from the pump chamber to the tank. The H_p block is to make sure flowrate is zero when the cam is not rotating.

4.3.2 Leakage Block

When the fuel pump is operating, a small amount of fuel will leak out through the tiny clearance between plunger and barrier wall. These leak fuels serve as a lubricant for the plunger and bushing to escape from the plunger spring chamber. [18]

According to (Zhao, 2012) [19], the amount of leakage through clearance can be calculated by:

$$q_{leak} = \mathrm{A}_{clrc} \cdot \mu\sqrt{2g\Delta h} \tag{4.28}$$

where A_{clrc} and Δh represent the sectional area of the clearance gap and pressure difference given by water head respectively, μ is the flow coefficient which can be found from the experimental data.[19]

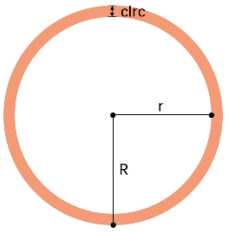

Figure 25. The area of a ring

The area of clearance is not a measurable parameter, so the length of clearance is used in this model to calculate the area of clearance. As illustrated in fig. 26, the area of clearance is calculated by:

$$\begin{aligned} \mathrm{A}_{clrc} &= \pi \cdot (R^2 - r^2) \\ &= \pi \cdot clrc \cdot (2r + clrc) \end{aligned} \tag{4.29}$$

Where, the radius of the smaller circle is the radius of the plunger: $r = \frac{D_P}{2}$.

The Simulink model is built accordingly:

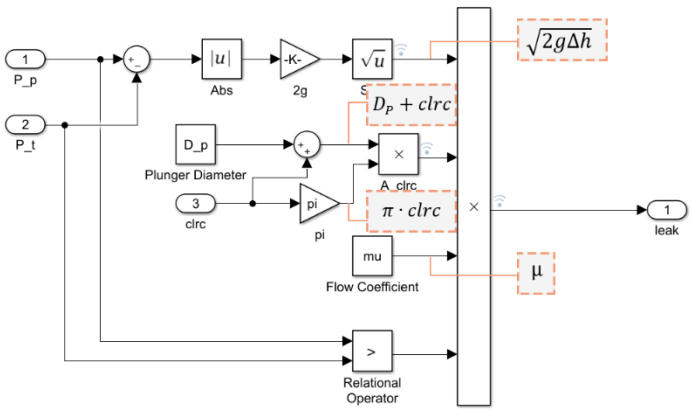

Figure 26. Model of leakage

4.3.3 'To Injector' Block

The 'to injector' block calculates the fuel flowrate supplied to the injectors, and the block consists of two sectors. As illustrated in Fig.23, the first sector is simulating the operation of a delivery valve. The delivery valve is a ball valve, which can be lifted by the fuel pressure. The first sector simulates the lift of the ball valve under the current pump pressure, and computes the effective sectional area of the ball valve based on the lift value, after which the second sector derives the value of effective area and computes the fuel flowrate to the injector.

Figure 27. Conceptual Model of the 'to injector' Block

Delivery Valve

The delivery valve is regard as a linear actuator to the pressure difference. It's assumed that the valve lifts to the maximum when pump pressure also at its maximum value. So, the lift of the delivery valve is:

$$\mathrm{H}_{dv} = \mathrm{H}_{dv\,\max} \cdot \frac{P_p - P_r}{P_{p\,\max} - P_r} \tag{4.29}$$

Where, P_r is the resistance force, P_p is the pump pressure, $P_{p\,\max}$ is the maximum pump pressure, $\mathrm{H}_{dv\,\max}$ is the maximum lift of the delivery valve.

Known the lift of the delivery valve, the effective opening area of a ball valve is considered as proportional to the lift:

$$\mathrm{A}_{dv} = \mathrm{A}_{dv\,\max} \cdot \frac{\mathrm{H}_{dv}}{\mathrm{H}_{dv\,\max}} \tag{4.30}$$

The Simulink block for the above equation is as follows:

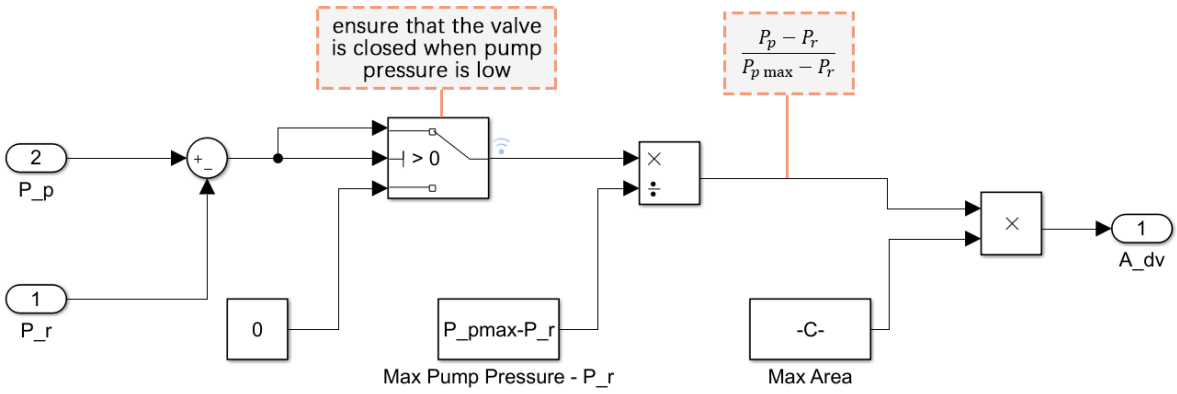

Figure 28. Layout of the lift calculation block

Fuel Flowrate to Injector

Substituting the effective area of the delivery valve A_{dv} to the generic flowrate function (3.1), the flowrate between the pump and the injector can be calculated:

$$q_{inj} = C_{di} \cdot A_{dv} \sqrt{\frac{2}{\rho} |P_{\mathrm{p}} - P_{\mathrm{r}}|} \tag{4.31}$$

Where, C_{di} is the discharge coefficient of the pump delivery port.

The corresponding Simulink model is built as below:

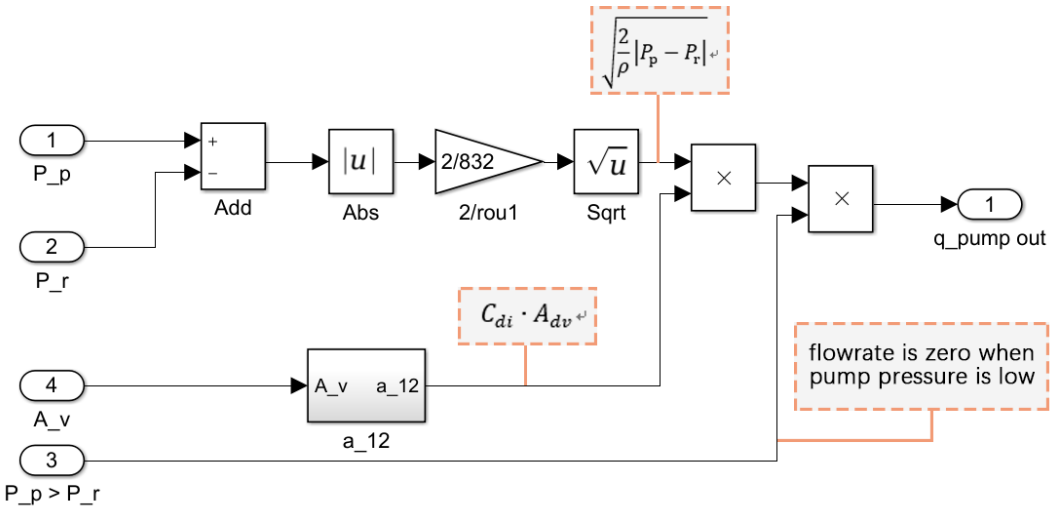

Figure 29. Layout of the Block Calculating Flowrate Supply to the Injector

Inputs for this section is the pump pressure P_{p}, the resistance pressure P_{r}, the effective area of the delivery valve A_{dv} and an extra signal ensuring the flowrate is zero when P_{p} is lower than P_{r}.

4.3.4 Pump Pressure

As all the flowrates comes in and out of the pump chamber has now been modelled, it's possible to start the modeling of the pump pressure. According to equation 4.4, the pump pressure is given by:

$$\dot{P} = \frac{K_f}{V_P}(Q_{in} - Q_{out} + \dot{V}) \tag{4.4}$$

Where, V_P is the simultaneous volume of the pump chamber, Q_{in} is calculated in the barrel model, Q_{out} are the sum of the 'leakage' model, the 'to injector' model and the 'barrel' model, and $\dot{V}$ the volume change due to cam movement are given by the movement of 'cam' model.

The overall pump model is configurated as below:

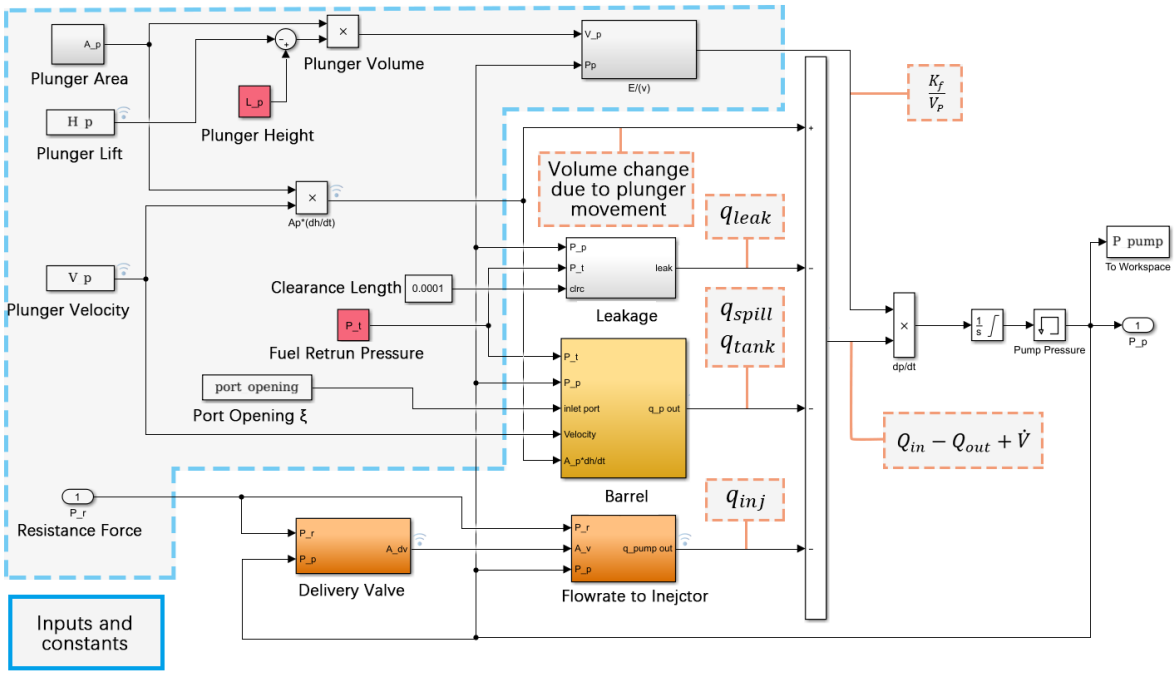

Figure 30. Pump Model

The operation results in Fig (31) shows that the pump pressure slowly increases when the plunger is moving upward, then ascend drastically after the inlet port is blocked. The pump pressure start falling when the blocking period finished. During the supplying phase, the pump pressure stays equal to the tank pressure:

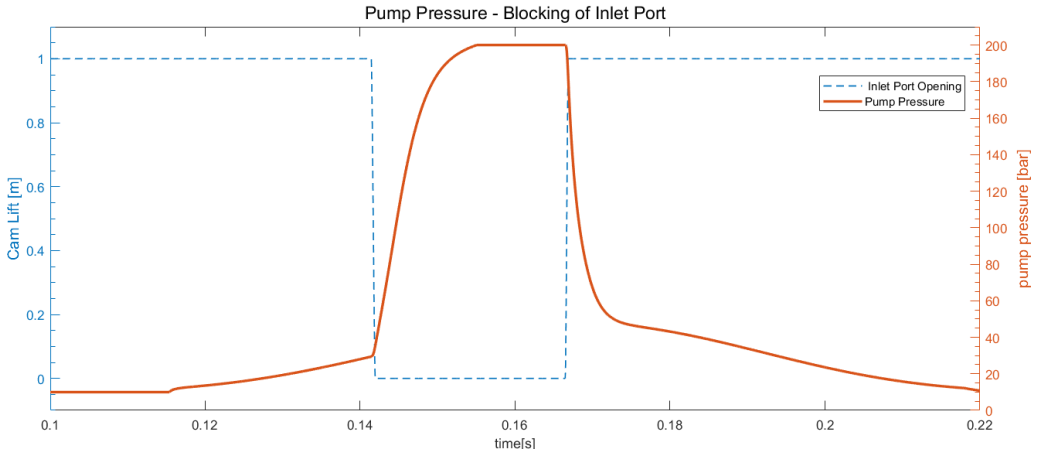

Figure 31. Operation Result of the Pump Pressure

4.4 Mechanical Injector

The needle valve of the mechanical injector is lifted by the supplied fuel from the high-pressure pump. The pressurized fuel from the pump are accumulating in the accumulation chamber of the injector, injection starts when the pressure in the accumulation chamber become large enough to overcome the spring force.

To simulate this process, the injector model firstly receives the fuel supplied rate q_p from the pump model as an input. The pressure in the accumulation chamber is calculated by:

$$\dot{P}_n = \frac{K_f}{V_n}(Q_{in} - Q_{out}) \tag{4.32}$$

Where, Q_{in} is equal to the supplied fuel q_p, Q_{out} is the amount of fuel injected into the cylinder; V_n is the volume of accumulation chambers in the injector.

The fuel pressure in the accumulation chamber P_n determines the movement of the needle valve. At the beginning of fuel entering the injector, the pressure starts building up and the needle valve is not lifted, no fuel is injected. As the pressure further increase, the needle valve is lifted up and the second-order differential equation governs the dynamic of the movement of the valve is:

$$m_n \ddot{x}_n = A_n \cdot P_n - b_n \cdot \dot{x}_n - K_n \cdot x_n \tag{4.33}$$

Where, m_n is the mass of the needle valve; A_n is the effective area of the needle valve that hydraulic pressure acting upon; P_n is the fuel pressure inside the accumulation chamber; b_n is the damping coefficient of the needle valve; K_n is the spring coefficient; x_n, $\dot{x}_n$, $\ddot{x}_n$ denotes the displacement, velocity and acceleration of the needle valve respectively.

The lift of the needle valve, on the other hand, determines the amount of fuel being injected into the cylinder Q_{out}, and consequently changes the pressure P_n. Reproducing the operation of the injector requires the model to simulate the interaction between the hydraulic pressure and the movement of the needle valve.

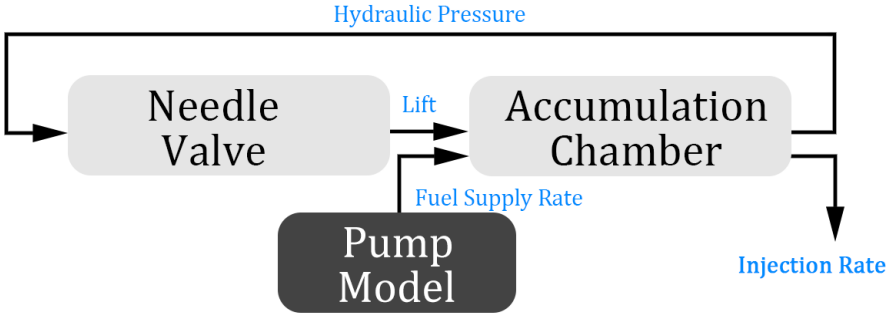

Figure 32. Conceptual Model of the Mechanical Injector

4.4.1 Fuel Pressure in the Accumulation Chamber

The accumulation chamber of the injector is a hydraulic chamber with single inflow and single outflow. As mentioned in function (4.32), the pressure of the accumulation chamber is given by:

$$\dot{P}_n = \frac{K_f}{V_n}(Q_{in} - Q_{out}) \tag{4.32}$$

Where, Q_{in} is the fuel supply rate calculated by the 'to injector' block of the pump model; Q_{out} is the injection rate.

The configuration of the accumulation pressure calculation block is as below:

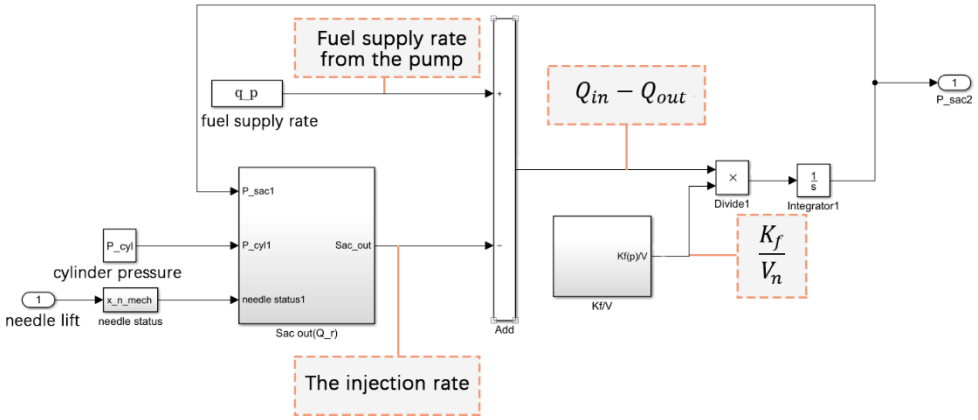

Figure 33. The Accumulation Chamber Block

Where, the q_p block is the supply rate derives from the plunger pump model. The needle lift is from the needle movement section, and controls the opening of the nozzle.

Q_{out}, the injection rate is calculated by:

$$Q_{out} = C_{d,cyl} \cdot A_{cyl}\sqrt{\frac{2}{\rho}|P_{\mathrm{n}} - P_{\mathrm{cyl}}|} \tag{4.34}$$

Where, $C_{d,cyl}$ denotes the discharge coefficient of the nozzle hole; A_{cyl} is the effective area of the nozzle holes; P_{n} is the fuel pressure in the accumulation chamber; P_{cyl} is the cylinder pressure.

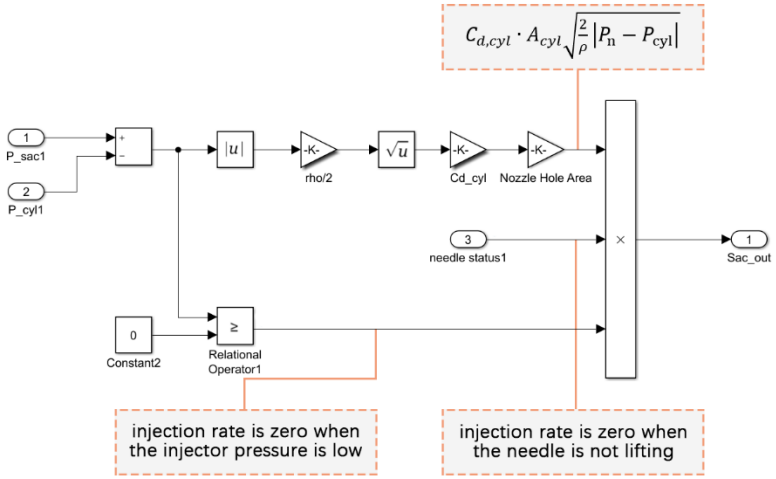

Figure 34. The Mechanical Injection Rate Calculation Block

4.4.2 Movement of the Needle Valve

There're three forces acting vertically upon the needle valve: the spring force, the damping force and the hydraulic force exerted by the pressure control chamber.

- The ***hydraulic force*** is calculated by:

$$\mathrm{F}_{hyd} = A_n \cdot P_n \tag{4.35}$$

Where, $\boldsymbol{A_n}$ is the sectional area of the needle; $\boldsymbol{P_n}$ is the pressure in the pressure control chamber;

- The ***damping force*** section is built in accordance to:

$$\mathrm{F}_d = b_n \cdot \dot{x}_n \tag{5.36}$$

Where, $\boldsymbol{b_n}$ is the viscous friction coefficient of the needle; $\boldsymbol{\dot{x}_n}$ denoteds the velocity of the needle.

- The ***spring force*** is calculated by:

$$F_s = K_n \cdot x_n \tag{4.37}$$

Where, $\boldsymbol{K_n}$ is the spring constant of the needle valve spring; $\boldsymbol{x_n}$ denoteds the displacement of the ball valve.

Consequently, the second-order differential equatial that governs the dynamic of the ball valve is given by:

$$\mathrm{m}_n\ddot{x}_n = A_n \cdot P_n - b_n \cdot \dot{x}_n - K_n \cdot x_n \tag{4.38}$$

Where, $\mathbf{m_n}$ is the mass of needle valve; $\boldsymbol{\ddot{x}_n}$, $\boldsymbol{\dot{x}_n}$, $\boldsymbol{x_n}$ denoteds the acceleration, velocity and displacement of the needle valve.

The model is structured as follows:

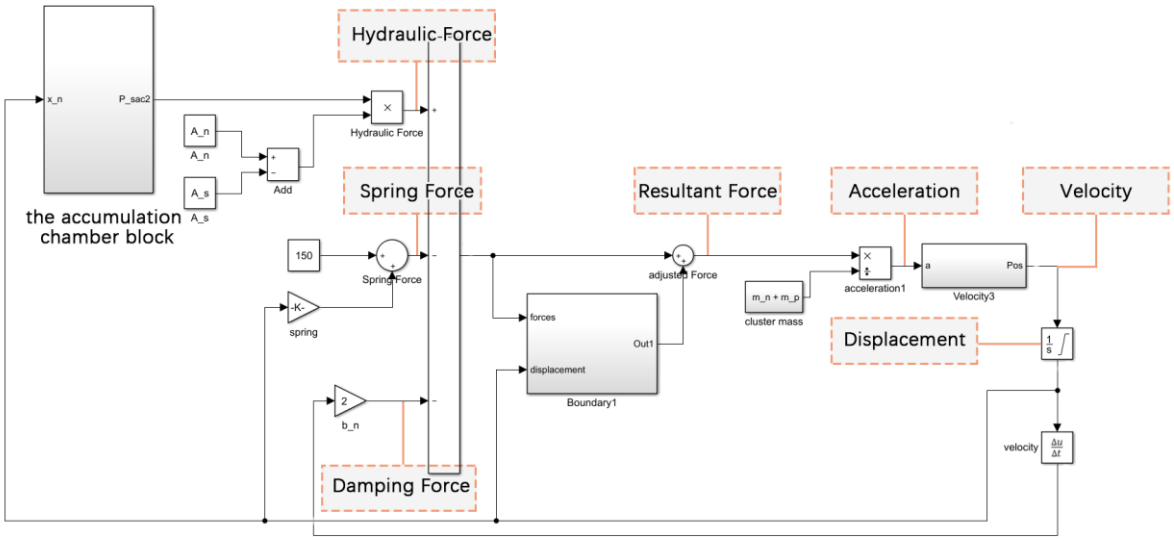

Figure 35. The Needle Valve Model(Mechanical Injection)

4.5 Summary

This chapter elaborated the development of a mechanical injection system model. Firstly, a cam model is developed to simulated the movement of the pump's plunger. The movement of the plunger changes the volume of the pump chamber, and subsequently the fuel pressure inside the pump.

Subsequently, a plunger pump model is built to simulate the pressure inside the pump chamber. The operational process of the plunger pump is divided into three phases: the supplying phase, the injection phase and the spilling phase, and three sub-blocks are built to calculate the flowrates at each phase. Additionally, the covering of the inlet port is reproduced in a seperated 'inlet port' model to increase the accuracy of simulation. Then the sum of the flowrates together with the volume change due to plunger movement determines the pressure inside the pump chamber.

Following by the pump model is the mechnical injector model, in which the injection rate and the injection pressure is simulated. The injector model is made up of a hydraulic chamber section simulating the fuel pressure and a needle movement section simulating the lift of the needle. The fuel pressure and the needle lift together determines the injection rate.

5

MODEL DEVELOPMENT: COMMON-RAIL INJECTION SYSTEM

In this chapter, the development of the high-pressure common rail injection system will be introduced. Both the configuration and the function of each segment in the model will be discussed in detail.

5.1 Configuration of the Common-Rail Injection System Model

Data shows that the pressure inside common rail is fluctuating on a very small scale.[10] Thus the CR injection model is built under the assumption that common rail is a constant pressure source, the main task is to simulate the working principle of a solenoid injector:

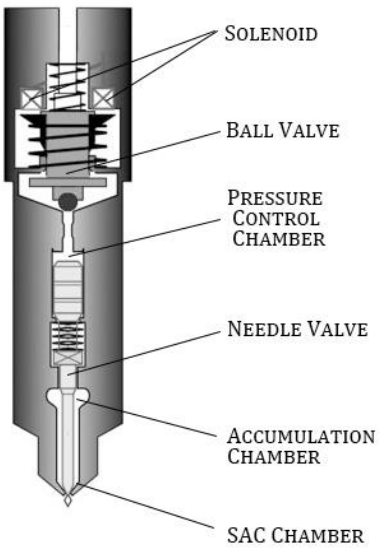

Figure 36. Solenoid Injector

The model consists of three tyeps of segment, which are the ***eletrical actuating components***, the ***mechanical valves,*** and the ***hydraulic chambers***.

The interaction between the segments can be summarized as a chain effect, which starts from the solenoid controls the opening of ball valve, and following by changing the pressure in pressure control chamber, then changes the lift of needle valve.

The model is configurated according to the chain interactions between components mentioned above:

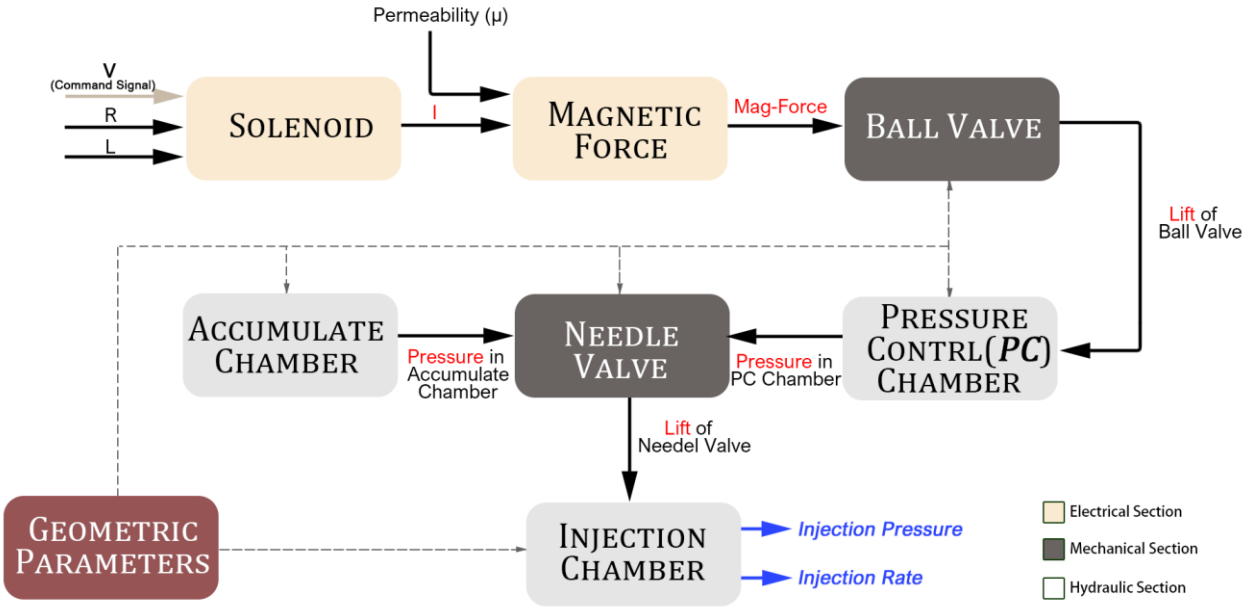

Figure 37. The Configuration of Common-Rail Injection System Model

The inputs for the common rail injection system model includes a command signal V and the geometric parameters of the relating components. The output is the injection pressure and the injection rate.

The CR injection model functions as follows: Firstly the *solenoid* derives a command voltage ***V***, gets energized and induces a current ***I***, then generates a magnatic force ***F_mag***. The magnatic force from solenoid pulls up the *ball valve* and opens the connection between the *pressure control chamber* and the drainage port, fuel in the pressure control chamber releases. As fuel released, the pressure in the *pressure control chamber* drops down as well; the *needle valve* then is being lifted up by the hydraulic pressure in the *accumulate chamber*, fuel injectes out through the *sac chamber*. The fuel pressure in the sac chamber is the injection pressure, and the fuel flowrate out of the sac chamber is the injection rate.

5.2 The Electrical Actuating Blocks

The electrical actuating blocks are the solenoid block and the magnetic force block. They are reponsible of calculating the magnetic force and controlling the injection timing. The movement of the ball valve is also initiated by the output from the magnetic force block.

5.2.1 The Solenoid

The solenoid is simplified as an RL circuit (Fig.38(a)). Because of the presence of inductance, current in the solenoid will not rise to its maximum value immediately when the voltage applies, as shown in Fig.38(b). The feature of inductance reproducing the respond delay in the real solenoids.

The response function of current in an RL circuit is [21]:

$$\mathrm{I} = \frac{E}{R} - \frac{E}{L \cdot \mathrm{d}i/\mathrm{d}t} \tag{5.1}$$

The RL circuit and it's current's change over time is dicpicted:

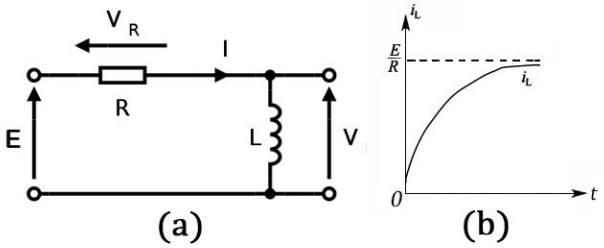

Figure 38. (a) The RL Circuit (b) The current-time Curve

The solenoid block calculates the current of the solenoid is structured as below: $\frac{E}{R}$

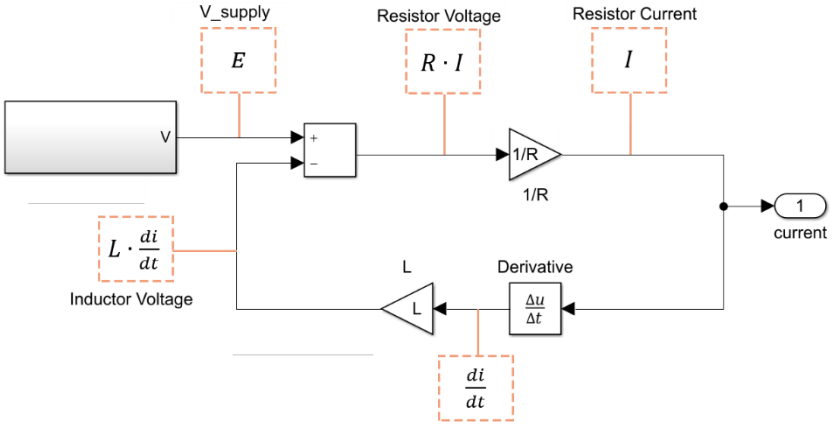

Figure 39. the solenoid block

$L \cdot \frac{di}{dt}$ In this model, the commanding voltage is a two-stage signal: the first stage is a short 60V impulse to lift the ball valve rapidly. The second stage is a 40V maintaining voltage lasting for the rest of the injection period. Opearting reslut shows an observable respondse delay of current due to the inductance:

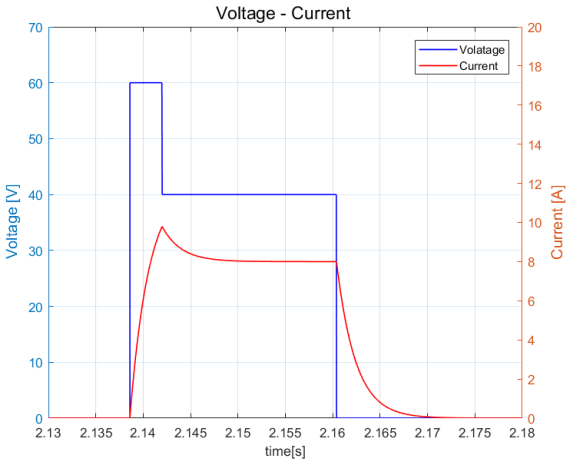

Figure 40. The Input Voltage and The Current Response of The Solenoid Model

5.3 Mechanical Valves

The mechanical elements, including the ball valve and the needle valve, were modelled as mass–spring–damper systems.

5.3.1 The Ball Valve

As shown in Fig.41, the ball valve controls the connection between the pressure control chamber and the valve chamber.

The valve chamber is connected to the fuel return line, so the fuel pressure inside it is the fuel return pressure P_t. When the ball valve is closed, the pressure in the pressure control chamber preserves at the rail pressure P_R.

Once the ball valve is open, the fuel pressure in the pressure control chamber P_c and the valve chamber P_v were equalized to the same pressure as the fuel return pressure P_t.

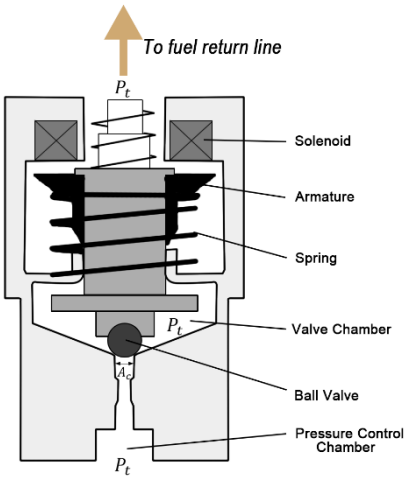

Figure 41. Scheme of the Ball Valve

There're four forces acting vertically upon the ball valve: the magnetic force, the spring force, the damping force and the hydraulic force exerted by the pressure control chamber.

- The ***hydraulic force*** is calculated by:

$$F_{hyd} = A_{pc} \cdot P_{pc} \tag{5.2}$$

Where, $\boldsymbol{A_c}$ is the area of orifice between the pressure control chamber and the valve chamber; $\boldsymbol{P_{pc}}$ is the pressure in the pressure control chamber;

- The ***damping force*** section is built in accordance to:

$$F_d = b_b \cdot \dot{x}_V \tag{5.3}$$

Where, $\boldsymbol{b_b}$ is the viscous friction coefficient of the ball valve; $\boldsymbol{\dot{x}_V}$ denoteds the velocity of the ball valve.

- The ***spring force*** is calculated by:

$$F_s = K_V \cdot x_V \tag{5.4}$$

Where, $\boldsymbol{K_V}$ is the spring constant of the valve spring; $\boldsymbol{x_V}$ denoteds the displacement of the ball valve.

- The ***magnetic force*** calculation is simplified into a propotional funtion of the current:

$$F_{mag} = A \cdot \mathrm{I} + \mathrm{B} \tag{5.5}$$

Where, **A** ad **B** are manually adjusted parameters; **I** is the current.

Consequently, the second-order differential equatial governs the dynamic of the ball valve is:

$$\mathrm{m}_V \ddot{x}_V = F_{mag} + A_{pc} \cdot P_{pc} - b_b \cdot \dot{x}_V - K_V \cdot x_V \tag{5.6}$$

Where, $\mathbf{m_V}$ is the mass of ball valve; $\ddot{\boldsymbol{x}}_{\boldsymbol{V}}$, $\dot{\boldsymbol{x}}_{\boldsymbol{V}}$, $\boldsymbol{x_V}$ denoteds the acceleration, velocity and displacement of the ball valve.

The Simulink model for the ball valve is as follows:

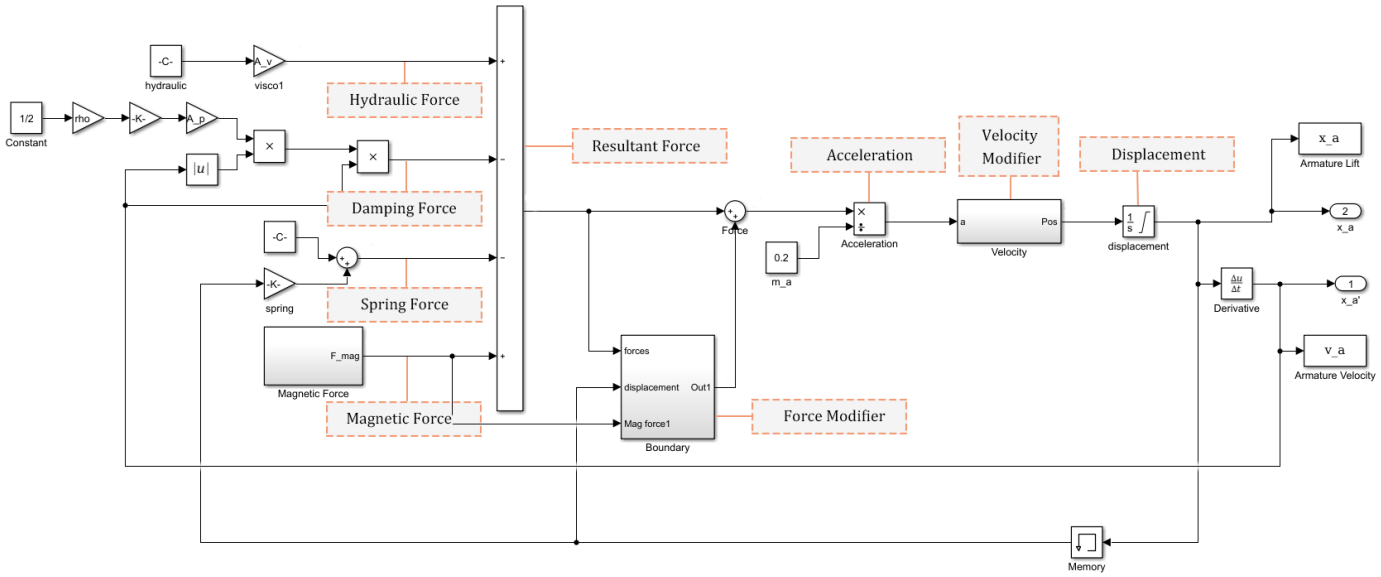

Figure 42. Block of Ball Valve

As shown as Fig.42, inputs for the block are the geometric coefficients of the ball valve and the pressure in the pressure control chamber; outputs are velocity and displacement of the ball valve.

Differ from the typical mass-spring-damping model, the ball valve model has its constraint on displacement. Hence, the resultant force will not always cause acceleration to the ball valve:

Table 6. Status of the Ball Valve

Position / Force Direction	Top end	Bottom end	Middle
Downward	YES	NO	YES
Upward	NO	YES	YES

The YES in the above chart reprsents the force will cause acceleration, and NO means the force will not cause acceleration.

The two circumstances that force doesn't cause acceleration are:

- The ball valve is at the top end, and the resultant force is acting upward;
- The ball valve is at the bottom end, and the resultant force is acting downward.

Under these two circumstances, the ball valve has no displacement change, zero velocity, and zero acceleration. If directly calculates the accleration, velocity and the displacement of the ball valve by consecutive integration, the operating results will not be wraped to zero under the two circumstances mentioned above. For this reason, some extra revise works are done to constraint the acceleration, velocity and the displacement output.

Revised Force

The resultant force is sent to the 'Boundary' block. The block is acting as a filter, finding out the circumstances that the resultant force needs modification by a series of logic judgements. The layout of the 'Boundary' block and the function of each element are shown as follows:

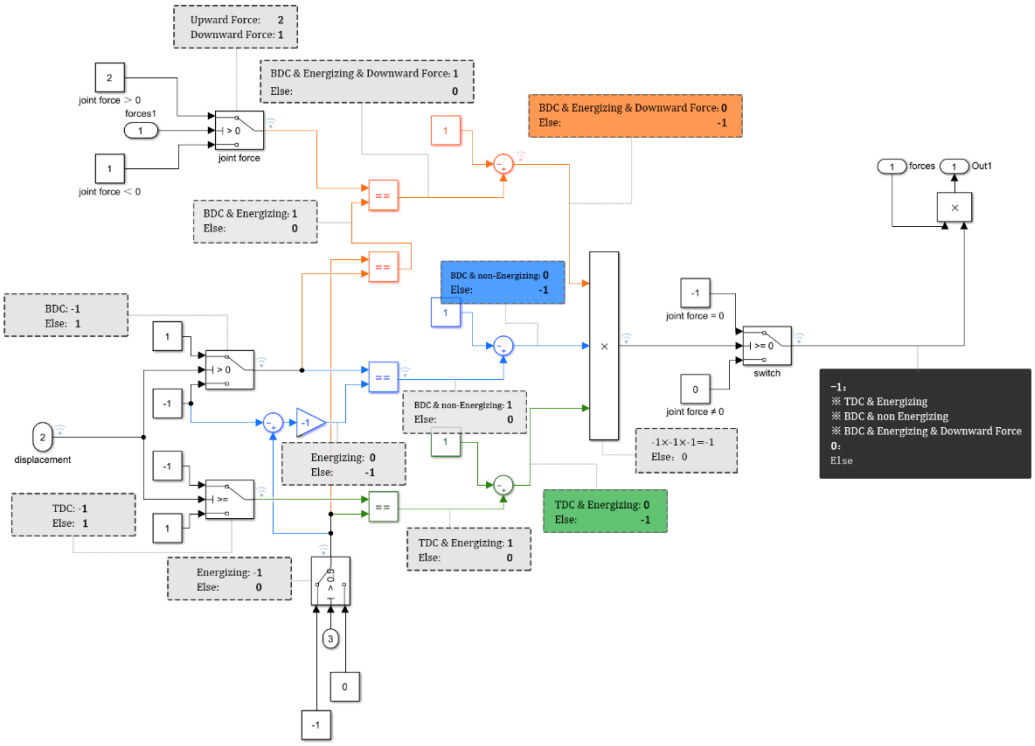

Figure 43: The Layout of the Force Modifying Block of the Ball Valve Model

When the final output is '**0**', the resultant force obtained from the preceding calculation is unaffected.

When the final output is '**-1**', the resultant force will be modified to zero. As illutrated in Fig.43, the conditions that resultant force will be warped to zero are:

- The ball valve is at the top end, and the solenoid is energizing;
- The ball valve is at the bottom end, and the solenoid is not energizing;
- The ball valve is at the bottom end, the solenoid is energizing, but the force is acting downward.

The former two are the two circumstances discussed already. The third one happens when the energizing process just started, during this short period the gradually increasing magnative force is smaller than the resistance force, so the reslutant force is acting downward even though the solenoid has been energized in this case. Therefore, the force needs modification since it doesn't bring about any acceleration to the ball valve.

Revised Velocity

As the acceleration is modified, the velocity still needs revise as simple integration calculation will keep the velocity at a constant value instead of wrapping to zero when the ball valve is not moving. The modification is done by a conditional judgement block as presented:

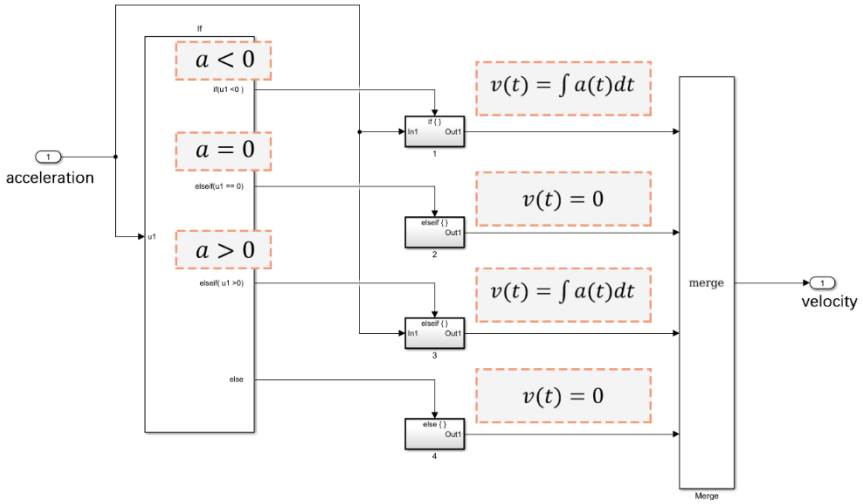

Figure 44. The Layout of Velocity Block

Revised Displacement

The constraints on displacement are realized by setting saturation limits on the integration block.

5.3.2 The Needel Valve

The control piston and the needle valve could be assumed to be a single clustered mass in the model. As can be seen in Fig.45, the needle valve integration has four forces acting upon: the spring force, the viscous friction, the hydraulic force from the pressure control chamber and from the accumulation chamber.

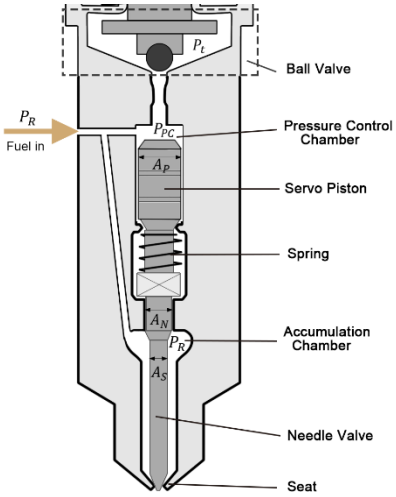

Figure 45. Scheme of The Needle Valve

- The ***hydraulic force*** from the pressure control chamber is calculated by:

$$\mathrm{F}_{pc} = A_{pis} \cdot P_{pc} \tag{5.7}$$

Where, $\boldsymbol{A_{pis}}$ is the area of the control piston; $\boldsymbol{P_C}$ is the pressure in the pressure control chamber.

- The ***hydraulic force*** from the accumulation chamber is calculated by:

$$\mathrm{F}_{ac} = (A_N - A_S) \cdot P_R \tag{5.8}$$

Where, $\boldsymbol{A_N}$ is the area of the bigger end of the needle valve; $\boldsymbol{A_S}$ is the area of the smaller end of the needle valve; $\mathbf{P_A}$ is the pressure in the accumulation chamber.

- The ***spring force*** is given by:

$$F_s = K_N \cdot x_N \tag{5.9}$$

Where, $\boldsymbol{K_N}$ denotes the spring constant of the needle valve spring; $\boldsymbol{x_N}$ denotes the displacement of the needle valve.

- The ***damping force*** is calculated by:

$$F_d = b_N \cdot \dot{x}_N \tag{5.10}$$

Where, $\boldsymbol{b_N}$ is the viscous friction coefficient of the needle valve; $\boldsymbol{\dot{x}_N}$ denotes the velocity of the needle valve.

Hence, The second order differential equation governs the dynamic behavour of the needle valve cluster is:

$$\mathrm{m}_N \ddot{x}_N = (A_N - A_S) \cdot P_p - A_{pis} \cdot P_{pc} - b_N \cdot \dot{x}_N - K_N \cdot x_N \tag{5.11}$$

Where $\mathbf{m_N}$ is the integrated mass of the control piston and the needle valve; $\boldsymbol{\ddot{x}_N}$, $\boldsymbol{\dot{x}_N}$ and $\boldsymbol{x_N}$ denotes the acceleration, velocity and displacement of the needle valve repectively.

The Simulink model of the needle valve is built accordingly:

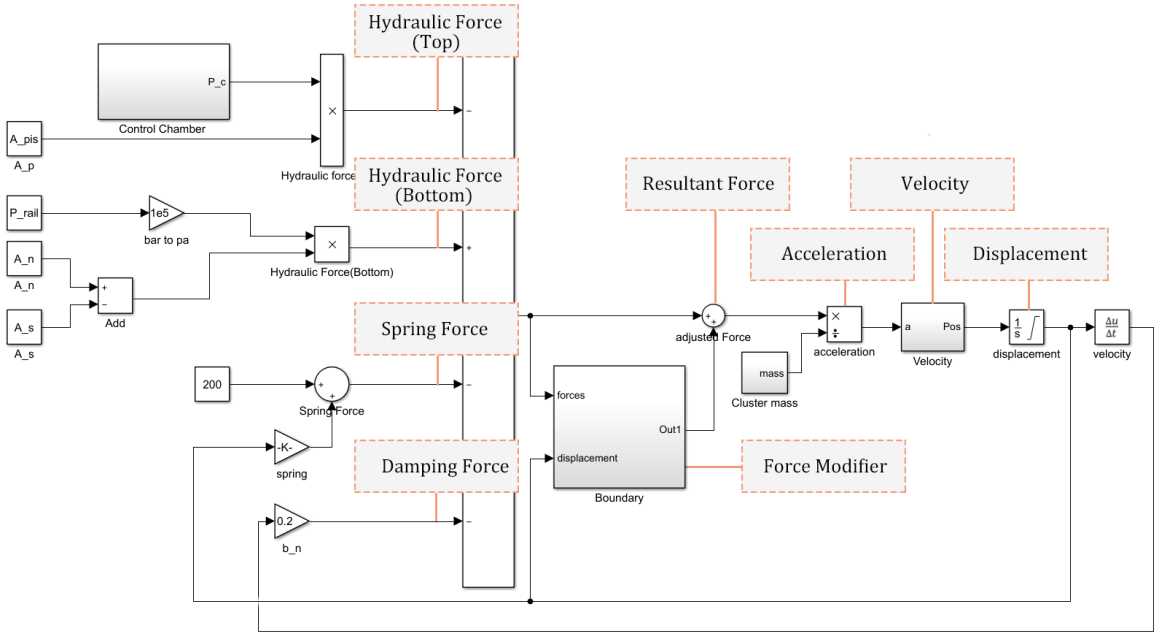

Figure 46. Configuration of the Needle Valve Model

Input for this model are the geometric parameters, and outputs are the velocity and displacement of the needle valve.

Similarly, the needle valve model is a mass-spring-damping model with displacement constraints. Therefore, some modification blocks are included to simulate the movement of the needle valve correctly.

Revised Force

The resultant force wounld not cause acceleration to the needle valve under two circumstances:

- The needle valve is at the bottom end, and the resultant force is acting downward.
  In this situaion, the needle valve is already againsting the seat, so the downwards resultant force wounldn't cause acceleration to the needle.
- When the needle valve is at the top end, and the resultant force is acting upward.
  In this situation, the needle valve has been fully lifted by the hydraulic pressure. The resutant force is still pushing the needle valve though; it doesn't cause any acceleration to the needle valve.

Under these two situations, the resultant force needs to be modified to zero. Otherwise, the succeeding integration block will generate a wrong result of accelration.

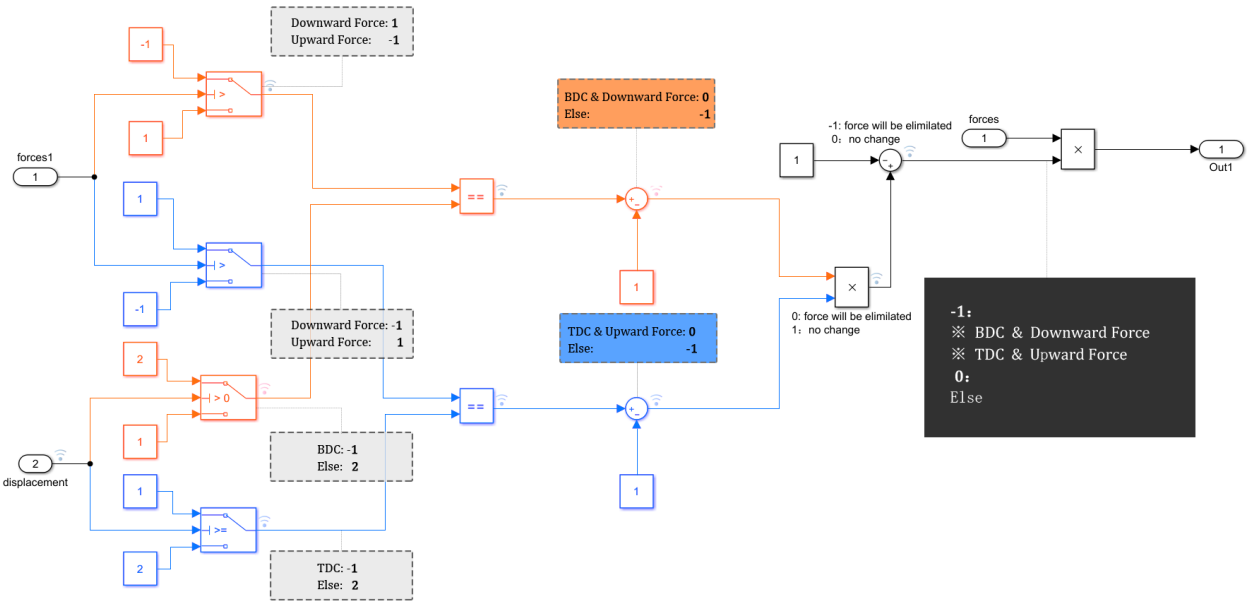

Figure 47. Configuration of the Force Filter Block of the Needle Valve Model

There are two inputs for the 'Boundary' block of the needle valve model: the position of needle valve and the direction of the resultant force. Using a series of logic judgement elements, the block can find out the two circumstances that resultant force needs wrapping to zero and output '**-1**'. When the final output is '**0**', the resultant force can pass through the boundary block unaffected.

The modifing process for velocity and displacement are identical to that in the ball valve model, which will not repeat here.

5.4 Hydraulic Chambers

The hydraulic chambers are the pressure control chamber, the accumulation chamber and the sac chamber. The former two are used to control the lift of the needle valve. The sac chamber is calculating the fuel pressure and flowrate injected into the combustion chamber.

5.4.1 Pressure Control(PC) Chamber

As shown in Fig. 48, the PC chamber is located above the servo piston, it receives fuel from the common rail, and releases fuel to the fuel return line when the ball valve is open.

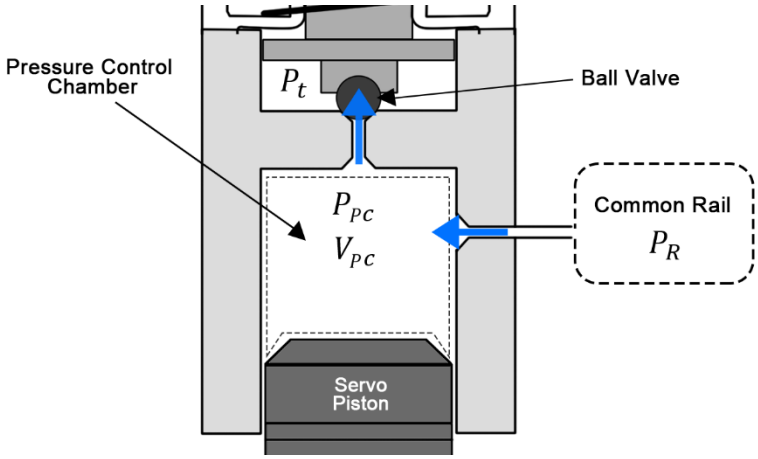

Figure 48. Scheme of the Pressure Control Chamber

Fuel pressure in the PC chamber P_c is equal to the rail pressure P_r when the ball valve is closed, and decreases to the fuel return pressure when the ball valve is open. Thus, pressure in the PC chamber is represented by a function of the ball valve's lift:

$$P_{pc} = P_r - (P_r - P_t) \cdot \frac{H_V}{H_{V\,max}} \tag{5.12}$$

Where, P_r, P_t denotes rail pressure and fuel return pressure; H_V is the lift of ball valve; $H_{V\,max}$ is the maximum lift of ball valve .

The PC chamber model is configurated as follow:

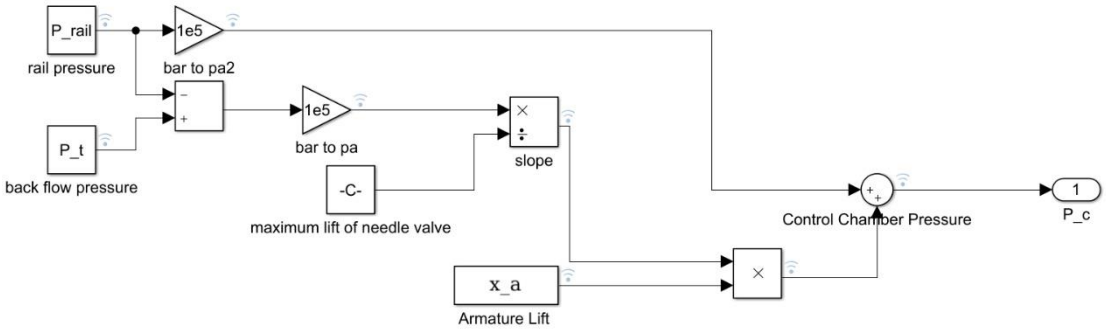

Figure 49. layout of PC chamber block

5.4.2 Accumulation Chamber

The accumulation chamber is connected to the common rail, thus the pressure inside is considered constant as the rail pressure.

5.4.3 Injection Chamber

The injection chamber is the volume surrounding the lower end of the needel. The volume of the injection chamber is not a constant. As dicpicted in Fig.50(B), the sac chamber becomes a part of the injection chamber during the injection.

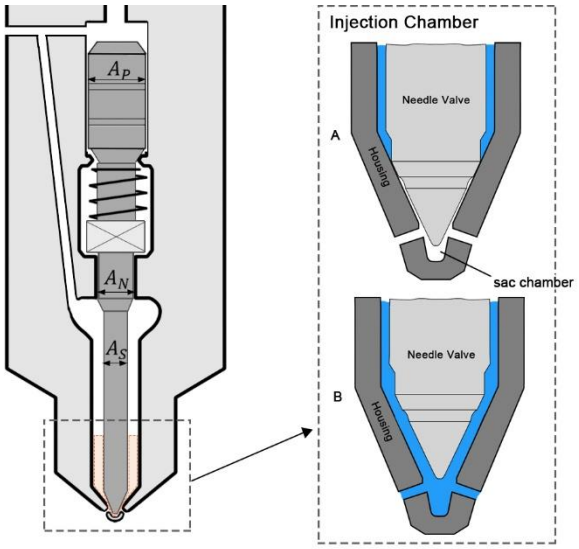

Figure 50. The Injection Chamber

Ideally, the change of chamber's volume due to movement of the needle valve should be the volume of the needle valve section leaving the injection chamber. But such a calculation would require detail geometric information of the needle, and will increase the complexity of the model to some scale. Therefore, the volume of the injection chamber is simplified as:

$$V_{ic} = V_{ic0} + A_N \cdot H_N \tag{5.13}$$

Where, V_{ic0} is the volume of injection chamber before the injection; A_N is the area of the bigger end of the needle; H_N is the displacement of the needle.

The pressure in the injection chamber is calculated by equation (5.14). (Chung, 2008) When there's no injection, the pressure in the injection chamber stays at the rail pressure. During the injection, as fuel leaving the chamber, the injection chamber's pressure drops down.

$$\mathrm{P}_{ic} = \frac{K_f}{V_{ic}}\left(Q_r - Q_{inj} + A_N \cdot H_N\right) \tag{5.14}$$

Where, Q_r denotes the fuel flow rate enters the injection chamber; Q_{inj} is the flowrate of fuel through the nozzle holes, also referred to as the injection rate; $A_N \cdot H_N$ is the volume change due to the needle movement

The volumetric flow rates of fuel are calculated by:

$$Q_r = C_{d\,i} \cdot A_i \sqrt{\frac{2}{\rho}|P_r - P_{ic}|} \tag{5.15}$$

$$Q_{inj} = \xi_n \cdot C_{d\,cyl} \cdot A_{cyl} \sqrt{\frac{2}{\rho}|P_{ic} - P_{cyl}|} \tag{5.16}$$

Where, C_{di} and C_{dcyl} are the discharge coefficient of the inlet and outlet orifice of the sac chamber respectively; A_i and A_{cyl} are the area of the inlet and outlet orifice of the injection chamber respectively; ξ_n is a binary number representing the opening of the nozzle determined by the needle lift, ξ_n when needle lift up to a threshold value.

The model of the injection chamber is configurated as follows:

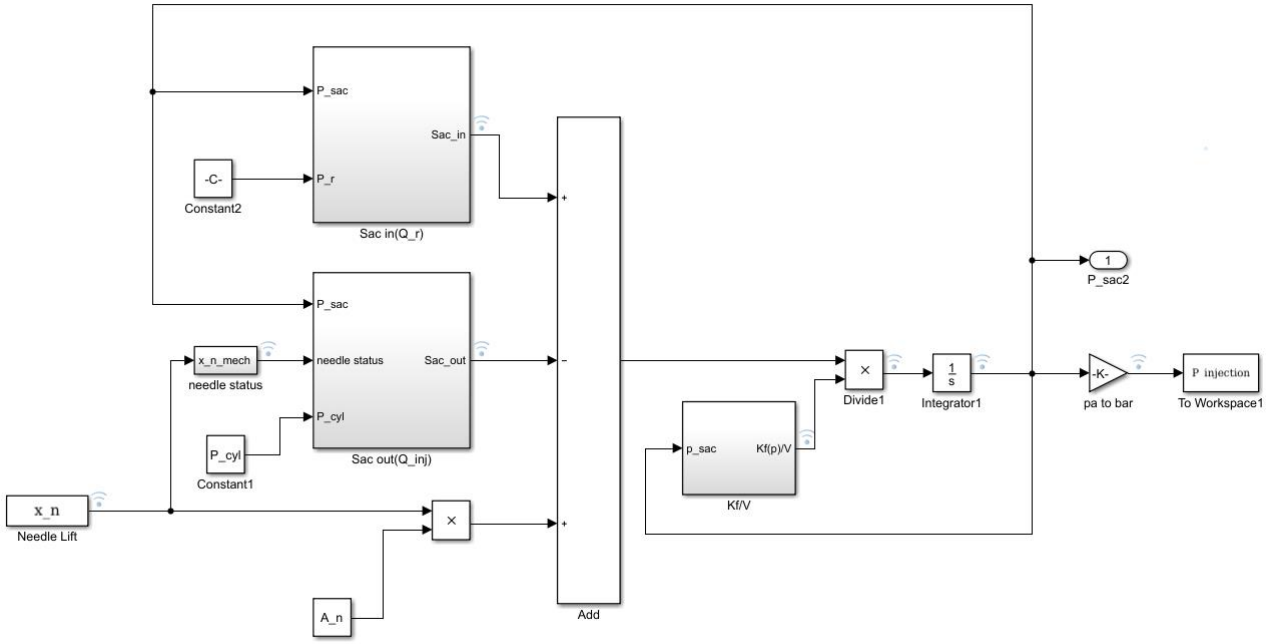

Figure 51. Layout of the 'Injection Chamber' Model

5.5 Summary

This chapter discussed the development of the electrical injector model. The electrical injector is considered made up of three types of basic sections: the electrical actuating components, the mechanical valves and the hydraulic chamber, and being functionalized by a sequentially linked effect which starts from the activation of the electrical solenoid.

The electrical solenoid is modeled as a Resistance-Inductance circuit, which receives the commanding signal and generates current, then the magnetic force to pull up the ball valve. The mechanical valves, including the ball valve and the needle valve, are both modeled as a mass-spring-damping system. In addition, three hydraulic chambers are taken into consideration in this thesis, and each of them is treated differently. The accumulation chamber is taken as a volume of constant pressure; The pressure inside the pressure control chamber is modeled as a linear function of the ball valve's lift; The injection chamber are simulated acccording to the 'hydraulic chamber' model.

6

MODEL VERIFICATION

6.1 Introduction

In the previous chapters, both the mechanical injection system model and the common-rail injection model have been developed. The remaining research sub-goal is to verify the simulation results. Ideally, the simulation data from both models should be verified based on the operation data from real engines. But in this thesis, only the results from the mechanical injection model are verified. The main reasons are:

1. Verification would require detail geometric data of the common rail injection system, while the published literature doesn't include sufficient geometric data to complete the verification.

2. No common-rail engine is available in the laboratory and the navy.

The verification of the mechanical injection model is carried out based on three relevant data:

- The geometric parameters of the cam.

- The Geometric parameters of the L20/27 injection pump and the flowrates of the pump at the fuel rack setting of 26mm and 23mm.

- The fuel consumption rate of a 4L20/27 MAN engine under various loads.

The main task of the verification is to verify the mechanical injector's injection rate under different loading conditions, based on the experiment data about the fuel consumption under various loads.

6.2 Verification of the Model

In a real engine, the adjustment on fuel injection is made by changing the fuel rack's position; The lateral movement of the fuel rack rotates the plunger and changes the effective length of the helix. The helix length determines the blocking period of the plunger pump's inlet port. Since the fuel can only be sent to the injector during the blocking period, the helix length determines the amount of fuel being injected per injection.

The fuel rack setting and the corresponding injection amount can both be found from the given data, while the length of the helix, which is the input of the model, is not mentioned by the data. Thus, the verification of the model starts from finding out the correlation between the fuel rack setting to the helix length. Then the model is able to simulate the injection amount when the helix length could be calculated. Next, the simulation results of injection amount will be compared to the real engine consumption data to finish the verification.

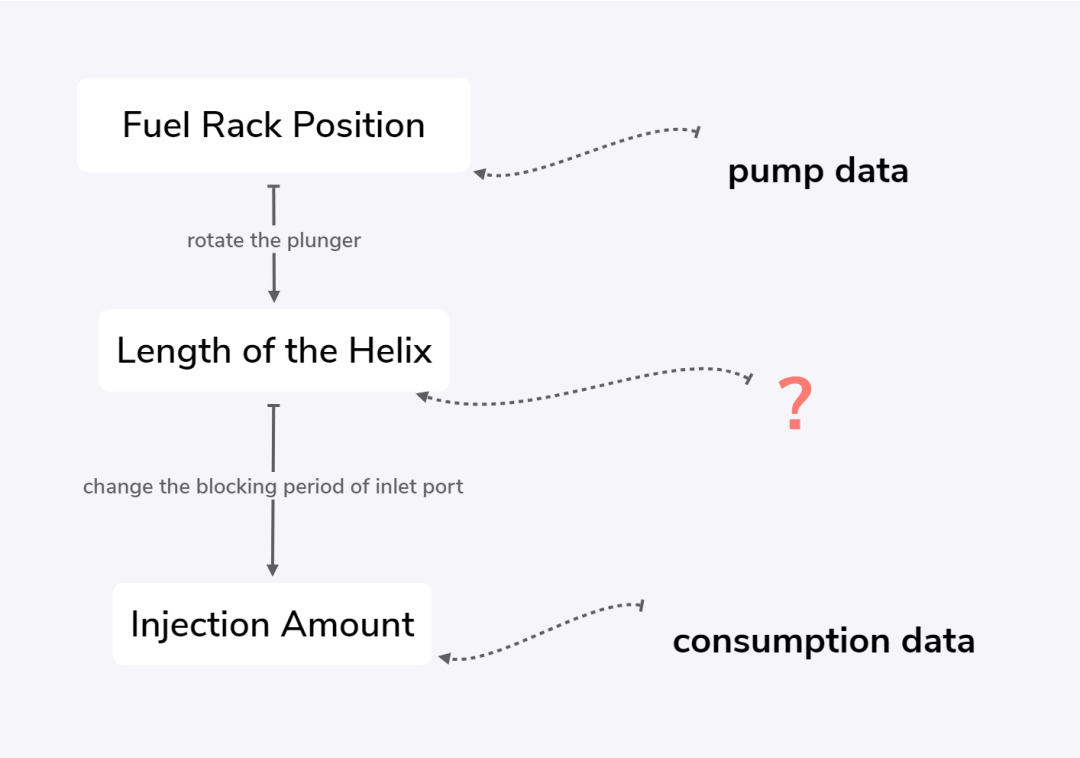

Figure 52.The scheme of Verification

6.2.1 Geometric Data and Experiment Results

To start with, the geometry parameters from the given data are put in the model. The geometric data for the pump and the cam is given below:

Table 7. Geometric Information of The Injection Pump and The Cam

				Units
Injection Pump		Type	L20/27	/
		Number of cylinders	1	/
	P_P	Pump Pressure	220	bar
	D_P	Plunger Diameter	27	mm
	L_P	Barrel Length	4	/
	n_P	Pump Rotation Speed	500	rpm
	clc	Clearance Length of the Pump Chamber		
Cam	H_C	Follower Lift/Pump Stroke	25	mm
		Angle of Start Rising	0	degree
	ϕ_r	Rise Angle	60	degree
	ϕ_h	High Dwell Angle	0	degree
	ϕ_f	Fall Angle	60	degree

The L20/27 pump is a cam- driven constant pressure single cylinder pump controlled by the lower helix, whose quantity of supplied fuel per pump stroke is varied by partial rotation of the plunger. The rotation changes the effective length of the plunger helix and subsequently the blocking period of the pump's inlet port, while the rotation of the plunger is achieved by the horizontal movement of the fuel rack. In this way, every fuel rack position has a corresponding helix length. Experiment on the injection pump shows the flowrates of the pump at two fuel rack settings:

Table 8. Flowrates of the Injection Pump

Fuel Rack	**Flowrate ($cm^3/200\ strokes$)**	**Flowrate ($m^3/injection$)**
Maximum (28 mm)	163	8.27E-07
23 mm	133	6.75E-07

However, the injection model requires the length of the helix to calculate fuel flowrate, but the correlation between the fuel rack position and the length of the helix is not given by the data. The following sub-section will focus on justifying the correlation.

6.2.2 Fuel Rack Position – Helix Length Correlation

The pump flowrates at two known rack positions are known from the previous section, in this section, we'll find the value of the helix length corresponding to the two given rack positions, and further estimate the overall correlation between the fuel rack position and the helix length.

To find out the actual helix length at fuel rack setting 28mm and 23mm, the model is operated with the helix length as an input. The helix length values where the operation result is identical to the given pump data are recorded as the real helix length:

Table 9. Helix Length at Two Fuel Rack Settings

Fuel Rack (mm)	**L_{hlx} (m)**	**Model Output (m^3/injection)**	**Pump Data (m^3/injection)**
23	4.46E-03	6.64E-07	6.65E-07
28 (Maximum)	5.23E-03	8.15E-07	8.15E-07

Based on the two known points, the correlation between the fuel rack position and the helix length are proposed in a linear way:

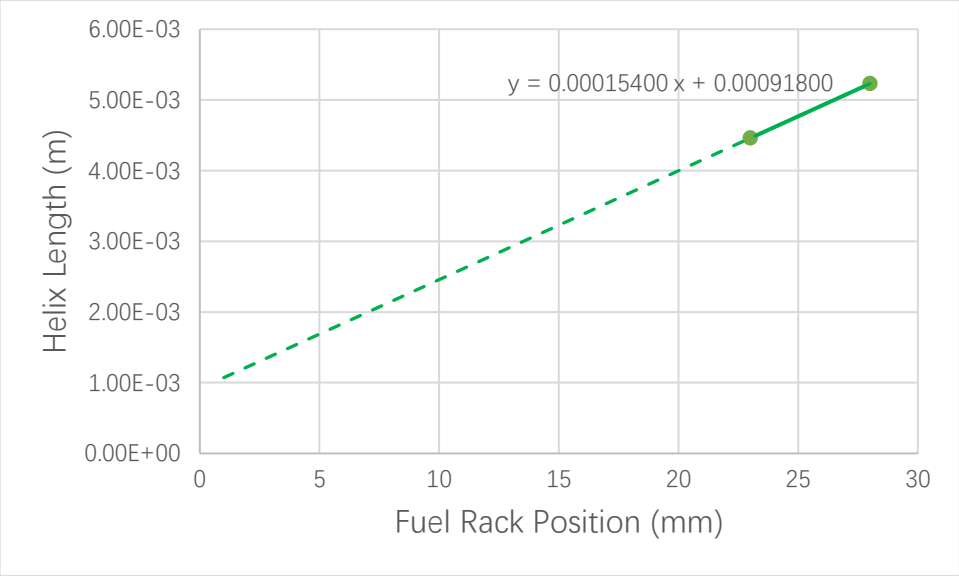

Figure 53. Helix Length-Fuel Rack Position Correlation Assumption

The equation of the forecast line is:

$$L_{hlx} = 0.000154 \cdot RACK - 0.000918 \qquad (6.2)$$

In the next section, Equation (6.2) will be used to determine the length of helix at different engine loading conditions.

6.2.3 Fuel Consumption Data

This section will focus on relating the experiment data to the pump's working condition.

The experiment data used for the model verification is derived from a test device as shown in Fig.53. The experiment device consists of a fuel tank, a test engine and two measuring devices. The diesel engine is of type 4L20/27 MAN, which has four injectors and one of the injectors is different from the others. The injection pressure is set at 140 bar. The engine itself equips an injection pump, the pump is of L20/27 type and driven by a cam.

The amount of fuel entering the engine was measured from the fuel tank, and the fuel being injected are measured after collecting from the injector, deviation between the two measuring results is the amount of leakage.

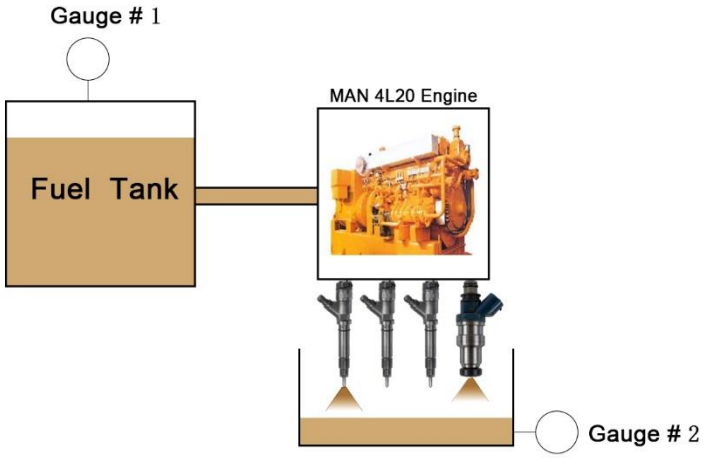

Figure 54. Experiment Device Setup

During the experiment, the engine is set to a certain power output to see how much time it takes to consume certain amount of fuel. The set points of this experiment are:

Table 10. Experiment Set Points

Set Point	N (rpm)	P (kW)	Loading (P/P_{max})	T (Nm)	Fuel (kg)	Time (sec)	Leak Fuel (g)
1	603	79.2	23.29%	1253	1	202	37
2	630	90	26.47%	1365	1	181	35
3	669	108	31.76%	1541	1	154	27
4	700	123.5	36.32%	1685	1	134	25
5	737	144	42.35%	1867	1	118	23
6	794	180	52.94%	2166	1.25	118	27
7	888	252	74.12%	2711	2	136	26
8	928	288	84.71%	2964	2	118	23
9	981	340	100.00%	3311	2.5	123	21

The geometric data of the injection system and relevant engine data are:

Table 11.Geometric Data of the Experiment Device

		Units
Number of cylinders	4	/
Injection pressure	140	bar
Diameter of Nozzle holes	2	mm
Volume of injector chamber	0.000003	m^3
Number of injectors	4	/
Engine type	Four stoke	

Note that the diameter of the nozzle holes and the volume of the injector chamber are not directly measured from the experiment engine due to lacking available data. Instead, the data are found from literature (Alkan Göcmen et al) [22] and are in a reasonable scale.

The measurement results are shown in table 12.

Table 12. Experiment Results

Set Point	Fuel injected (including leaked fuel) (kg/sec)	M_f: Fuel injected (not including leaked fuel) (kg/sec)	$m_{f,e}$: Fuel injected per injection (not including leaked fuel) (kg /inj)
1	4.95E-03	3.12E-03	6.16E-05
2	5.52E-03	3.59E-03	6.58E-05
3	6.49E-03	4.74E-03	7.28E-05
4	7.46E-03	5.60E-03	8.00E-05
5	8.47E-03	6.53E-03	8.62E-05
6	1.06E-02	8.31E-03	1.00E-04
7	1.47E-02	1.28E-02	1.24E-04
8	1.69E-02	1.50E-02	1.37E-04
9	2.03E-02	1.86E-02	1.55E-04

The data used for verification is the amount of fuel injected per injection (the 4th column), which is obtained by divided the injected fuel per second M_f by the firing frequency:

$$m_{f,e} = \frac{2 \cdot M_f}{rps \cdot n_{cyl}} \tag{6.3}$$

Where, M_f denotes the amount of fuel injected without the leakage; $m_{f,e}$ is the amount of fuel injected per injection, the subscript 'e' represents the data from the experiment; n_{cyl} is the number of cylinders, for this engine the cylinder number is four.

Referring to Table.13, the maximum flowrate of the pump and the injector is:

Table 13. Maximum Flowrate of the Pump and the Injector

Fuel Rack	Flowrate ($m^3/200\ strokes$)	Flowrate (m^3/injection)	Flowrate ($kg/injection$)
Maximum (28 mm)	1.63e-6	8.15E-07	6.78E-04

The loading condition of the pump at each experiment set point, which defined as the ratio of current injection rate to the maximum flowrate, are shown in table below:

Table 14. Loading Condition of the Pump

Set Point	$m_{f,e}$: Fuel injected per injection (kg/injection)	$m_{f,e}$: Fuel injected per injection (m^3/injection)	Injected Fuel / Max Flowrate
1	2.37E-04	2.85E-07	34.98%
2	2.54E-04	3.05E-07	37.44%
3	2.83E-04	3.41E-07	41.78%
4	3.12E-04	3.75E-07	45.99%
5	3.37E-04	4.05E-07	49.70%
6	3.92E-04	4.71E-07	57.75%
7	4.90E-04	5.89E-07	72.32%
8	5.42E-04	6.51E-07	79.88%
9	6.16E-04	7.41E-07	90.90%

The fuel rack setting at each set point are calculated by multiplying the maximum fuel rack to the pump loading:

Table 15. Fuel Rack Position and the Helix Length at Each Experimental Set Point

Set Point	Engine Loading (P/P_{max})	Pump Loading (Injected Fuel / Max Pump Flowrate)	Fuel Rack Position (mm)
1	23.29%	34.98%	9.793906567
2	26.47%	37.44%	10.48350581
3	31.76%	41.78%	11.69942056
4	36.32%	45.99%	12.87656808
5	42.35%	49.70%	13.91692926
6	52.94%	57.75%	16.17045717
7	74.12%	72.32%	20.24853585
8	84.71%	79.88%	22.3653159
9	100.00%	90.90%	25.4507602

In the next section, the model will calculate the fuel injection amount using the fuel rack position as an input. The operation results of injection amount from the model are compared to the actual experiment data to finish the verification.

6.2.4 Simulation Results from Mechanical Injection Model

At this point, the fuel rack setting at each engine operation point is known. But the model uses the helix length L_{hlx} to calculate the injected fuel. Luckily, the co-relation between the engine's fuel rack position to the pump's helix length has been investigated:

$$L_{hlx} = 0.000154 \cdot RACK - 0.000918 \quad (6.2)$$

By substituting the 'Fuel Rack Position' value to equation(6.2), the helix length at each operation point is obtained. The amount of injected fuel calculated by the model is shown in Table.16:

Table 16. Model Output of Helix Length and the Injection Amount

Set Point	Fuel Rack Position(mm)	Helix Length (mm)	Model Output (m^3/injection)	Experiment Data (m^3/injection)
1	9.793906567	2.42626	2.62E-07	2.85E-07
2	10.48350581	2.53246	2.88E-07	3.05E-07
3	11.69942056	2.71971	3.24E-07	3.41E-07
4	12.87656808	2.90099	3.60E-07	3.75E-07
5	13.91692926	3.06121	3.91E-07	4.05E-07
6	16.17045717	3.40825	4.60E-07	4.71E-07
7	20.24853585	4.03627	5.82E-07	5.89E-07
8	22.3653159	4.36226	6.45E-07	6.51E-07
Pump data 1	23	4.46000	6.64E-07	6.69E-07
9	25.4507602	4.83742	7.38E-07	7.41E-07
Pump data 2	28	5.23000	8.15E-07	8.15E-07

Plotting of the operation results (Fig. 55) shows a good matching to the experiment data, with only a slight deviation happens on the small fuel rack settings.

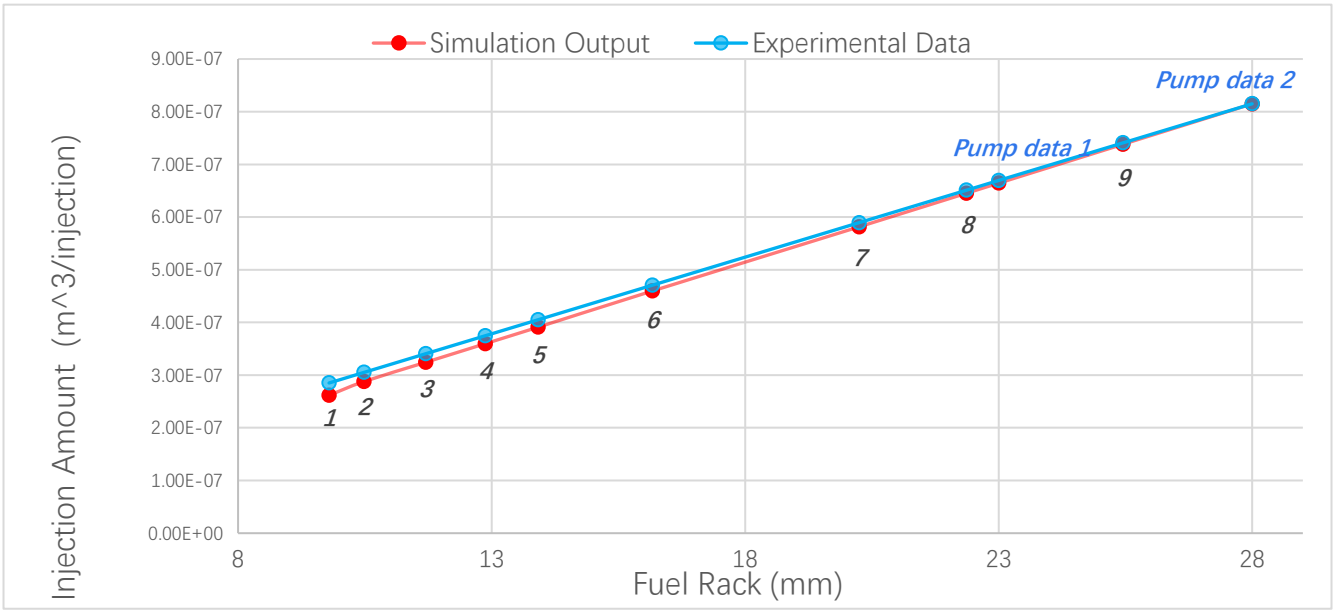

Figure 55. Operation Result and the Experiment Data

7

SIMULATION AND RESULTS

In this chapter, the simulation results of the two injection models will be addressed. The mechanical injection part will start by analyzing the fuel pump model, as the cam part has been addressed in chapter 3. The common rail injection part simulates how the commanding signal controls the injection, the whole procedure of fuel injection will be discussed. In addition, different injection strategies are also simulated in the common rail injection model by varying the commanding signal.

7.1 Mechanical Injection Model

The modeling results of the mechanical injection system are demonstrated in two subsections: ***fuel delivery*** and ***fuel injection***. The pressurizing and delivery of the fuel are simulated by the plunger pump model and the fuel injection by the injector model.

7.1.1 Simulation Results of Fuel Delivery

The pump's pressure starts increasing when the plunger is moving up. As shown in Fig. 56, the building up of pump pressure can be divided into two phases, with the first phase being a smooth rising followed by a drastic boosting phase due to the blocking of the inlet port.

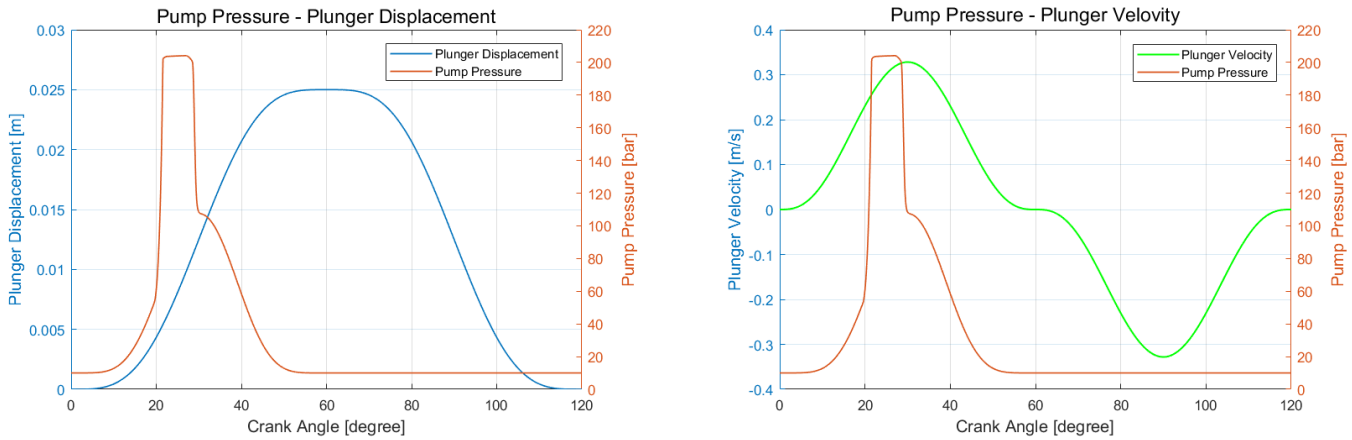

Figure 56. The Pump Pressure Changing with Follower Displacement

The declined of the pump pressure is also a two-phase procedure: the rapid decrease happens when the inlet port just revealed, as the huge pressure difference between the pump and the tank forces fuel out of the pump chamber rapidly. As the pressure further decreased, the pressure difference becomes smaller, plus the fact that the plunger's velocity also decreases, the pressure decline thus slows down to a smooth curve.

Pump Flows

The fuel flows in the pump chamber is modeled by three sub-blocks: the barrel model, the leakage model and the 'to injector' model. The following figure shows how the fuel is flowing inside the pump chamber when the pump is operating:

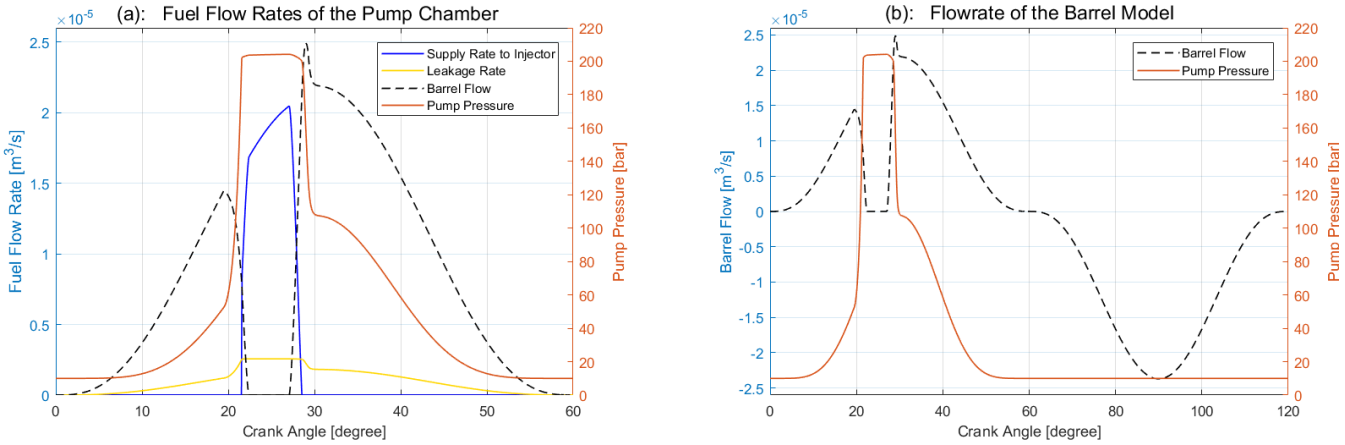

Figure 57. Fuel Flows in the Pump Chamber

- q_{brl}: Flowrate of the Barrel Model (fuel intake and spilling)

  The black dash line shows the flowrate between the pump chamber and the fuel tank. During the upward stroke of the plunger, the barrel flow is positive, which means the fuel is flowing from the pump chamber to the tank and the flowrate is the spilling rate. The spilling stops when the inlet port is blocked by the plunger, and starts again after the inlet port is revealed. The end of blocking causes a strong outflow where the barrel flowrate reaches the maximum value due to the high pressure in the pump chamber.

  The barrel flow becomes negative when the plunger starts moving down, which means the fuel is flowing into the pump chamber from the tank. For the sake of simplicity, the intake flowrate of pump is set equal as the increment of the volume of the pump chamber due to the plunger movement in this model, in this way the pressure fluctuation caused by fuel intake can be neglected, and the pump pressure stays equal as the tank pressure during the downward stroke of the plunger.

- q_{leak}: Leakage Rate

  The Leakage rate is relatively small, but happens the entire upward stroke of the plunger. The leakage amount increases along with the pump pressure.

- q_{inj}: Supply Rate to The Injector

  The flow rate supply to the injector happens simultaneously with the pressure boost, and stops a short moment after the inlet port revealed.

  As shown in Fig (58), due to the operational principle of the plunger pump, the fuel supply rate from the pump does not stay at a constant value when the inlet port of the pump is fully blocked. Instead, the fuel supply rate keeps increasing during the supplying phase, and the value of the supply rate is determined by the velocity of the plunger.

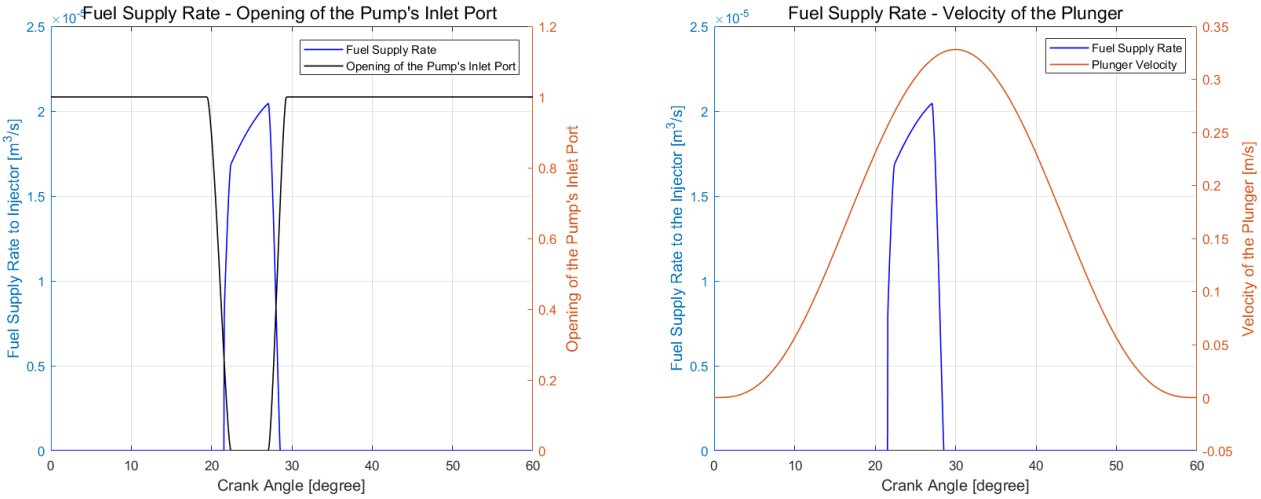

Figure 58. Fuel Supply Rate from the Pump Regarding to the Port Opening and Plunger Velocity

7.1.2 Simulation Results of Fuel Injection

Operation results in Fig (59) shows the process of needle lifting. (a): When the injector receives fuel from the plunger pump, the pressure inside the injector starts increasing immediately. (b): The needle being lifted up until the pressure in the injector is sufficient to overcome the resistance force from the spring.

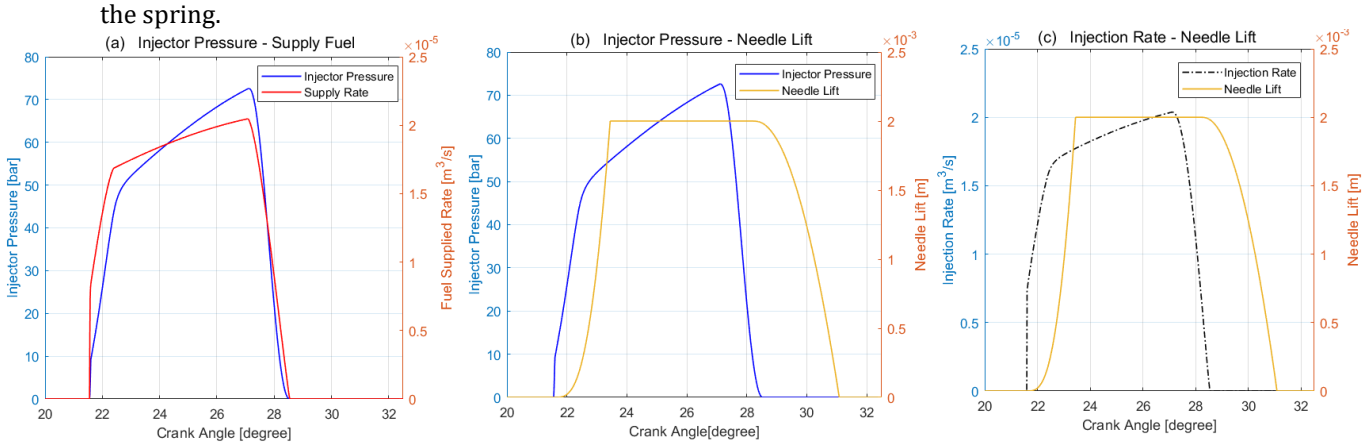

Figure 59. The Change of Injector Pressure and Needle Lift due to Fuel Supplied

Fig (59.c) shows the change of injection rate regarding the lift of needle valve. The lift of needle controls the effective area of the injection hole, higher needle lift results in a higher injection rate. Injection starts immediately when the needle is lifted, but the closing of needle valve happens much later than the injection finished.

A modelling error can also be observed from the simulation results that the needle valve does not fall to the seat immediately when the injection finished. The error is due to the restoring force from the spring being too weak. However, if the spring force is adjusted to a higher value, the operation result of the injection rate will oscillate at the beginning of pressure build up (Fig(60).c), and the injection pressure will also stay at a constant value during the injection rate oscillation (Fig(60).b).

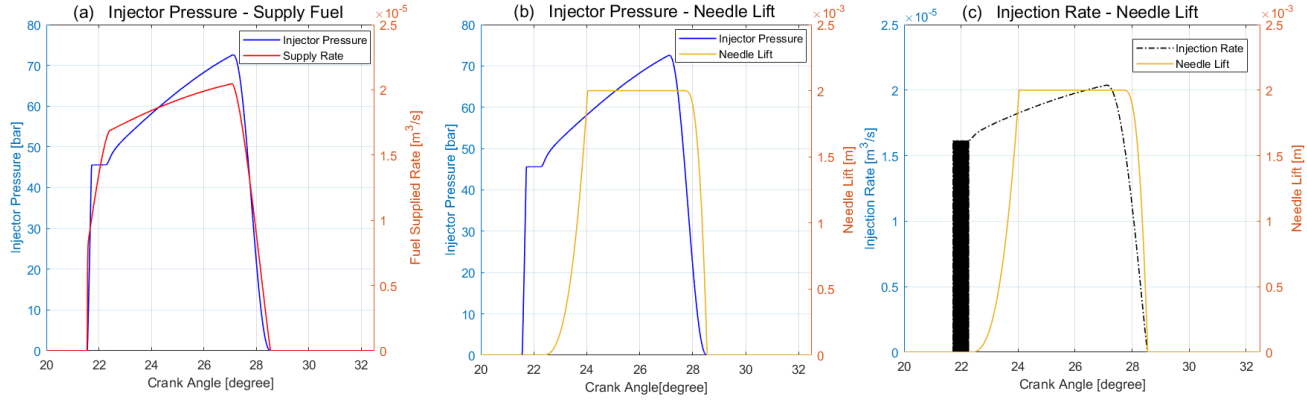

Figure 60. Operation Results of Fuel Injection at Spring Constant K=750

The oscillation in the fuel injection rate is because of the needle suffering large resistance force when it's lifting, so instead of a smooth lifting, the needle is vibrating near its seat. It's also observed that the injector pressure at which the injection rate oscillation happens is exactly large enough to counter the resistance force. So it's assumed that a simulation loop (Fig (61)) occurs during the oscillation period,

that once the needle is lifted up a bit, fuel injection will start and leading the injector pressure to decrease, and the decrease of injector pressure will close the needle valve, therefore will end the fuel injection, then the injector pressure arise again and start the loop.

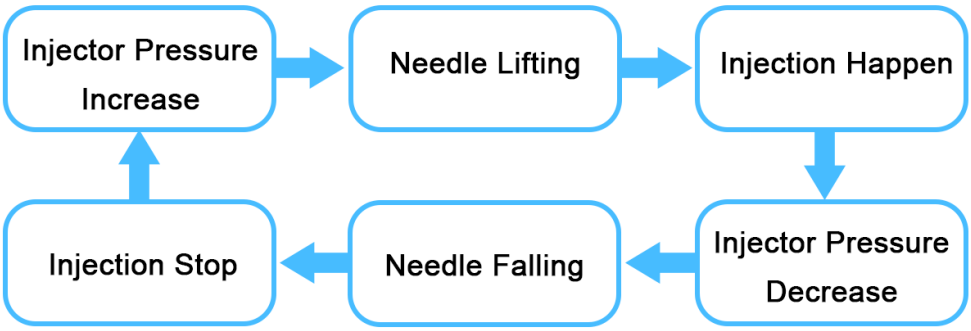

Figure 61. The Simulation Loop that Leads to the Injection Rate Oscillation

The operation also shows that the injection rate is obviously determined by the fuel supply rate. Due to the operational principle of the plunger pump, the fuel supply rate from the pump is not a constant, thus the fuel injection rate also keeps increasing when the needle valve has lifted to the maximum position. The injection rate is expected to stay at a maximum value when the needle is fully open if an additional fuel tube model is applied to even the supply flow.

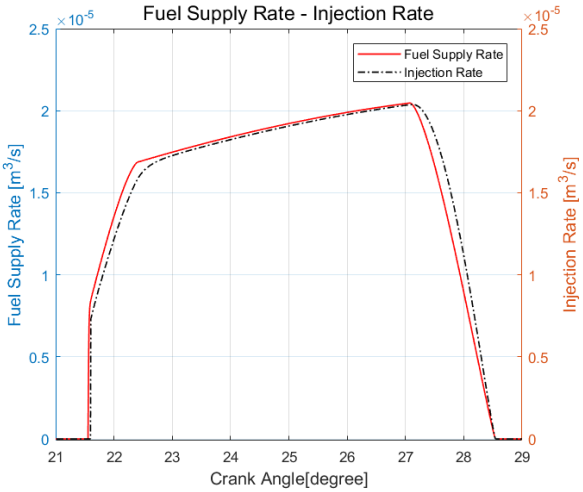

Figure 62. The Injection Rate and Supply Rate of the Injector

7.2 Common-Rail Injection Model

The simulation of the common rail injection system shows how the common rail injection model manages to realize a single fuel injection in accordance with the two-stage commanding voltage.

The model starts from simulating the electrical components. Firstly, a voltage pulse is sent to the solenoid model and generates current. The current in the solenoid exerts a corresponding magnetic force to pull up the ball valve. The process of magnetic force generation is depicted in Fig (63):

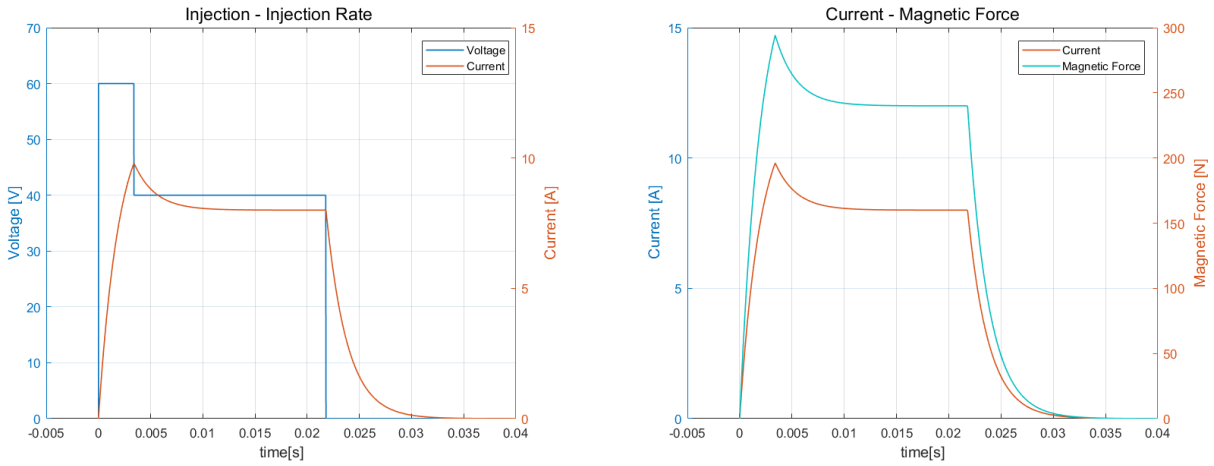

Figure 63. Commanding Voltage and Current, Magnetic Force Response

In this model, the commanding voltage is a two-stage signal: the first stage is a short 60V impulse to lift the ball valve rapidly. The second stage is a 40V maintaining voltage lasting for the rest of the injection period. Opearting reslut shows an observable respondse delay of current due to the inductance. The magnetic force is modeled as proportional to the current.

The magnetic force controls the pressure in the pressure control chamber by pulling the ball valve, once the ball valve is open, the pressure in the pressure control chamber drops down from the rail pressure to the tank pressure. Fig (64) shows the response of the pressure control chamber sub-block and the ball valve sub-block:

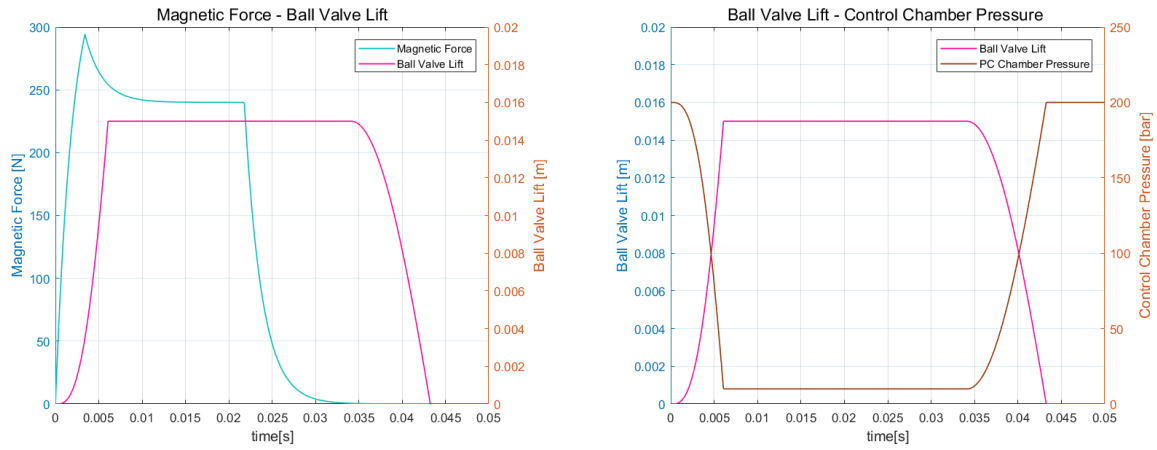

Figure 64. Ball Valve and PC Chamber Response to the Magnetic Force

As the pressure in the PC chamber drops down, the needle valve is pushed up by the hydraulic force from the accumulation chamber, whose pressure kept constant at the rail pressure. The lifting of the needle valve is illustrated in Fig(65):

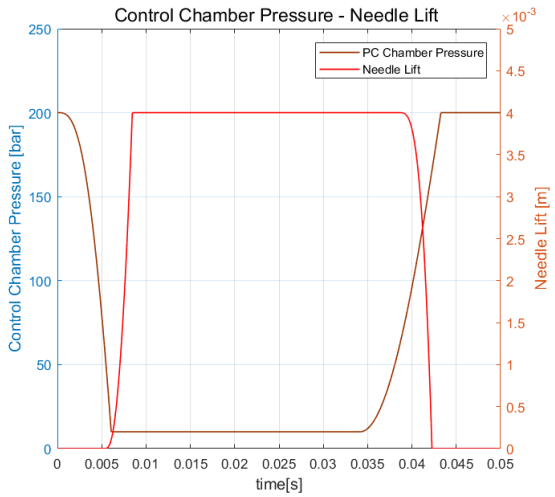

Figure 65. Needle Lift in Response to PC Chamber Pressure

The lifting of the needle valve unblocks the injection holes and initiates injection. The operation results of the injection process are shown below:

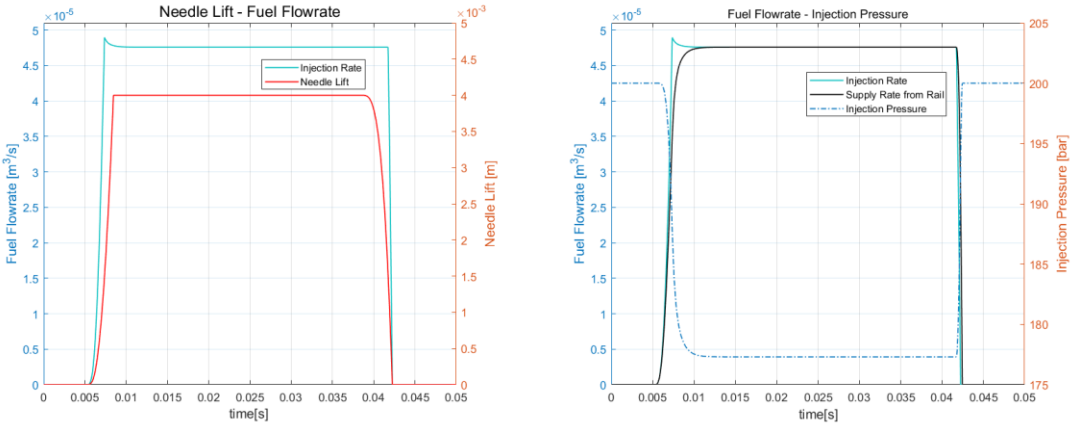

Figure 66. The Injection Process of the Common Rail Injection System

Some futures are found from the operation results:

- The injection rate reaches the maximum value within a very short time, even before the needle valve is fully lifted.
- The shape of the injection rate is not smooth. An apparent spike appears at the beginning of injection, and the end of injection is a straight cut off.
- During the injection, the pressure in the injection chamber decreases.
- The start and ending of injection process are strictly in accordance with the lifting of the needle valve.

The response speed for the common rail injection systems is defined as the time interval from receiving the signal to the start of injection. Comparing to the mechanical injector, the electrical injector has a more complex configuration which acquires the linked sequence of sections to realize the fuel injection and might lengthen the response interval. But simulation results show that the injection starts rapidly (within 0.005s) after receiving the commanding signal, which means that the complexity of the electrical injector doesn't slow down the response speed very much.

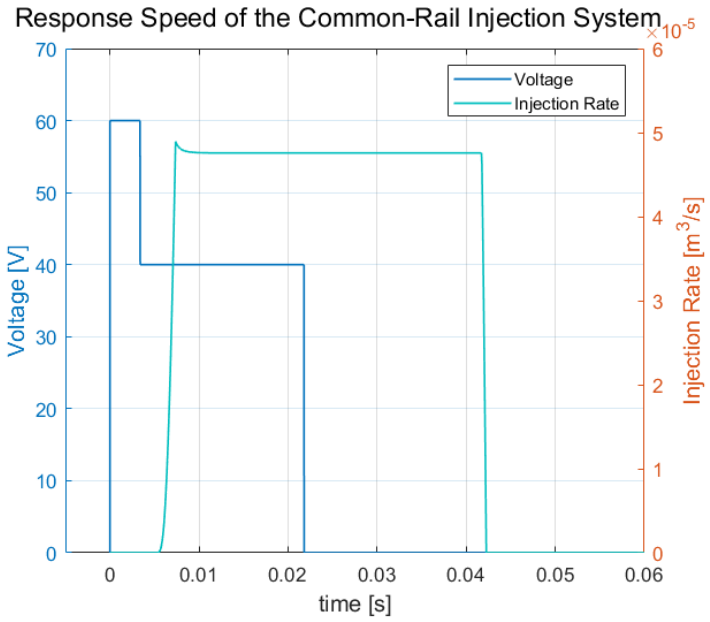

Figure 67. The Response Speed of the Common-Rail Injection Speed

8

CONCLUSIONS AND RECOMMENDATIONS

8.1 Conclusion

The main objective of this master program is to develop a model which capable of reproducing the injection process of the diesel engines. To achieve this goal, a literature study has been performed investigating the operation principle and the modeling methodology of the injection systems. In this project, the injection systems are considered consist of two basic elements:

- The hydraulic chambers: All the hollow chambers that contain fuel are modeled as a hydraulic chamber to calculate the chamber pressure and fuel flowrate.
- The mechanical valves: All the mechanical valves in the injection system are modeled as a mass – spring – damping system that has a lower and upper boundary.

Based on the two basic modeling elements, this thesis shows the development of a mechanical injection system model and a common rail injection system model.

8.1.1 Model Development

The mechanical injection system model reproduces the conventional injection mechanism. Firstly, a cam-driven injection pump model is developed to simulate the process of the fuel pressurizing and supplying, consisting of a cam model and a plunger pump model. In addition, an inlet hole model has been developed as a separated part of the plunger pump model to allow adjustment on the injection amount. Next, a mechanical injector model is developed to simulate the process of fuel injection, outputs the injection rate and the injection pressure. The interaction between the fuel pressure accumulation and needle lift is simulated using an inter-connected injection chamber model and a needle movement model.

The common rail injection model focus on the reproducing the behavior of an electrical injector. The model consists of a solenoid model, a ball valve model, a needle valve model and an injection chamber model. The four sections of the common rail model are run sequentially to simulate the process from receiving the electrical signal to fuel injection.

8.1.2 Simulation Results

The simulation results reveals the difference between the two injection systems:

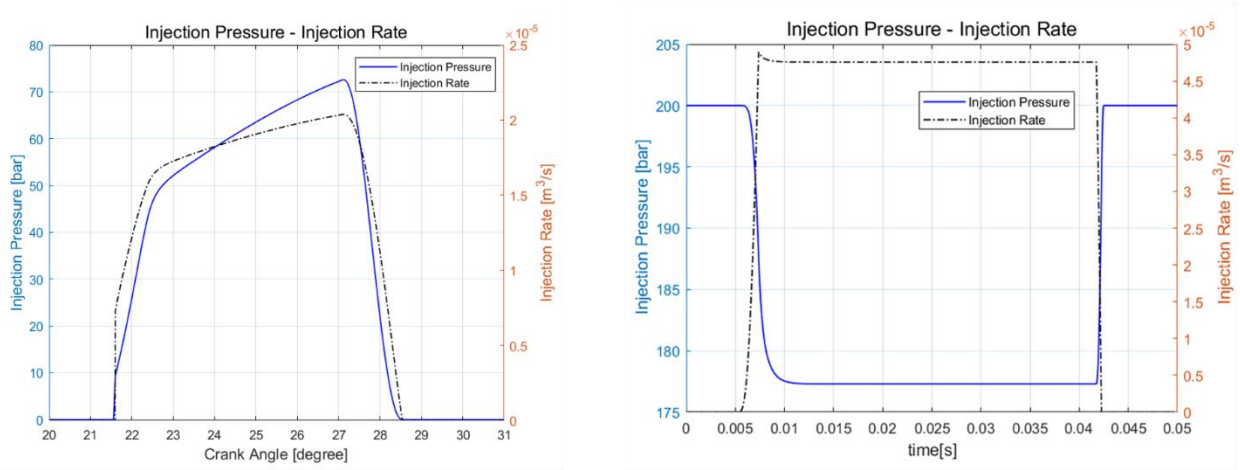

(a) Simulation results of mechanica injection (b) Simulation results of common-rail injection

Figure 68. Simulation Results of the Two Injection System Models

Simulation of the mechanical injection system shows that the injection rate is a smooth curve being shaped by the plunger's movement. The simultaneous injection rate is decided not only by the injection pressure by also by the plunger's moving speed. The pressure in the injection chamber increases during the injection.

But for the common rail injection system, the curve of injection rate is very steep, means that the start and end of the injection happen rapidly. The pressure in the injection chamber drops down during the during injection. The two simulations together show that the common rail injection system can react faster and more precise than the mechanical injection system.

The characteristics of each injection system that revealed by the simulation are summarized in the following table:

Table 17. The Characteristics of the Two Injection Systems

	Mechanical Injection	Common-Rail Injection
Start of Injection	Injection starts after the inlet port of plunger is blocked and determined by the cam angle.	The injection is initialized by the commanding voltage.
Injection Rate	The injection rate is shaped by the movement of the plunger, and peaks smoothly during the injection	The injection rate increases to the peak rapidly during injection and maintains at the maximum value.
End of injection	The injection rate smoothly decreases to zero and injection stops.	The injection rate stays at the maximum value until the needle valve is shut down.
Injection Pressure	The pressure in the injection chamber is zero when there is no injection , and increases during the injection.	The pressure in the injection chamber maintains at the rail pressure when there is no injection , and decreases during the injection.

8.2 Recommendations

In this section, the recommendations for further improvement on the model development are discussed. The recommendations will be elaborated in three parts. The first part gives recommendations about the research boundary, as some assumptions have been made in this thesis to limit the research boundaries, and some of the assumptions, however, will sacrifices the accuracy of modelling results thus needs improvement. The second part and the third part will list up the recommendations for further development of mechanical injection system and the common-rail injection system respectively.

Research Boundaries

- The change of fuel temperature due to pressurizing should be considered in the future injection system models. The temperature of fuel affects the density of fuel, and subsequently, change the injection pressure and injection rate.
- The collision of mechanical valves to the frame are considered fully inelastic in this model, that the force, velocity, and acceleration are all set to zero the moment when the mechanical valves reach the boundary. Further research is advised to use the impulse to simulate the movement of mechanical valves so that the valves don't stop immediately when the collision happens.

Mechanical Injection System Model

- In this thesis, the mechanical model is built as a combination of separate sub-models. In this way, different sub-models are not connected very well, especially for the plunger pump model and the injector model. The plunger pump model feeds only the supply rate to the injector model, so the injection pressure becomes somehow not affected by the pump supply pressure. For the future research, I advised to integrate the plunger pump model and the mechanical injection model into a single model, the pressure in the injection chamber should be used to calculate the pump supply rate.
- During the graduation program, the geometric parameters and constants such as the spring factor and the damping factor have always been lacking. Most of the needed constants are either found from literature or manually set. The parameters are the main source of modelling deviation. So for the further research, it's advised to start based on a real injection system, from which all the needed values can be directly measured. In this way, the accuracy of the injection models can be largely improved.
- A fuel tube model is needed for the mechanical injection system model. Because of the absence of the fuel tube model, the injection rate is directly shaped by the supply rate from the pump, which the flowrate keeps increasing when the needle valve is fully open. The fuel tube model is expected to even the supply rate from the pump, so the injection rate can maintain at a constant value when the needle valve lift to the top end.
- If the fuel tube model is introduced, future researchers can also investigate the pressure fluctuation, also known as the pressure wave, inside the fuel tube. After which an advantage of the common rail injection system, that can damp out the pressure fluctuation from the pump, can be validated by the model.

- The model built in this thesis fails to give an accurate simulation on the lift of the needle valve. The needle valve falls to the seat apparently later than the end of injection. This could be possibly solved by the correct setting of spring constants and the injector geometries.

- Future researchers can use the fuel rack setting, which easier to measure, as the input to the mechanical injection model.

Common-Rail Injection Model

- The common rail is set as a constant pressure source in the model. Future research can define the common rail as a chamber with limit volume and constant intake flow. A spill port can be introduced to maintain the common-rail pressure in the designated value. In this way, the pressure fluctuation in the common-rail can be well modeled and makes the injection system model more accurate.
- The magnetic force in this thesis is not calculated from formulas but set as a linear function to the current. The future researchers can refer to literature and calculate the magnetic force more realistically.
- The common-rail injection system is not validated in this thesis due to lack of available literature and experiment engines. Further investigations are therefore essential to validate the results and improve the model accuracy, especially when it comes to the integration with other systems.
- The common-rail injection system model is capable of realizing all the injection strategies by varying the commanding voltage setting. The model thus can be integrated with the in-cylinder combustion model to predict emission and heat release.

BIBLIOGRAPHY

[1] Khair, Magdi K.(2010), *Pump-Line-Nozzle Injection System*, Web.10 June.2010 https://www.dieselnet.com/tech/diesel_fi_pln.php

[2] United Diesel (2007), http://www.uniteddiesel.co.uk/docs/faqs/nozzle-set-up-di-page-2-1398762715.pdf

[3] Paolo Lino et al (2007), 'Nonlinear modelling and control of a common rail injection system for diesel engines', *Applied Mathematical Modelling*, 1770-1784

[4] Bosch Common Rail System https://aviondemand.com/shop/uncategorized/common-rail-diesel-crd-seminar/

[5] N-H Chung, B-G Oh, and M-H Sunwoo (2008), 'Modelling and injection rate estimation of common-rail injectors for direct-injection diesel engines', *Proc. IMechE Vol. 222 Part D: J. Automobile Engineering*

[6] D, T, Hountalas et al. (1998), 'Development of a fast and simple simulation model for the fuel injection system of diesel engines', *Advanced in Engineering Software* Vol. 29

[7] T. Sokolowski, K. Gerke, M. Ahmetoglu, T. Altan (2000), 'Evaluation of tube formability and material characteristics: hydraulic bulge testing of tubes', *Journal of Materials Processing Technology,* Vol. 98, Issue 1, 34-40

[8] R Payri et al. (2004), 'Diesel injection system modelling; Methodology and application for a first-generation common rail system', *Proc. Instn Mech. Engrs,* Vol. 218 Part D: J. Automobile Engineering

[9] J. N. Anno, J. A. Walowit and C. M. Allen (2011), 'Load Support and Leakage from Microasperity-Lubricated Face Seals', *J. of Lubrication Tech,* 91(4), 726-731 (Oct 01, 1969) (6 pages)

[10] Jun Feng Zhao et al (2014), 'On-Board Fuel Property Identification Method Based on High-Pressure Common Rail Pressure Signal', *Journal of Dynamic Systems, Measurement, and Control*, Vol. 136

[11] SABAU et al (2012), 'Modeling of High-Pressure Fuel Injection Systems', Annals of DAAAM for 2012 & Proceedings of the 23rd International DAAAM Symposium, Volume 23, No.1, ISSN 2304-1382

[12] X.L.J. Seykens, L.M.T. Somers and R.S.G. Baert (2004), 'Modelling of Common Rail Fuel Injection System and Influence of Fluid Properties on Injection Process', *Proceedings of VAFSEP2004*

[13] neutrium.net. (2015, 2 11). DISCHARGE COEFFICIENT FOR NOZZLES AND ORIFICES. Retrieved from neutrium: https://neutrium.net/fluid_flow/discharge-coefficient-for-nozzles-and-orifices/

[14] M.I.Arbab et al(2013), ‘Fuel properties, engine performance and emission characteristic of common biodiesels as a renewable and sustainable source of fuel’, *Renewable and Sustainable Energy Reviews,* Volume 22, June 2013, Pages 133-147

[15] "Bulk Elastic Properties". *hyperphysics. Georgia State University.*

[16] Shen Haosheng, Zhang Jundong and Cao Hui, 2014. ‘Visualization Simulation Research of Fuel Common Rail System of Marine Intelligent Diesel Engine’. *Information Technology Journal,* 13: 1648-1655.

[17] Aan A., Heinloo M., Allas J., 2014. Design of A Radial Cam for The Cam-Follower Mechanism. *9th International DAAAM Baltic Conference, "INDUSTRIAL ENGINEERING"*

[18] DISCHARGE COEFFICIENT FOR NOZZLES AND ORIFICES,15 Feb 20, https://neutrium.net/fluid_flow/discharge-coefficient-for-nozzles-and-orifices/

[19] W.Zhao et al (2012), ‘Study on the leakage flow through a clearance gap’, IOP Conference Series: Earth and Environmental Science, Volume 15, Part 2

[20] R.T. S. Ferreira and D. E. B. Lilie, 1984. Evaluation of the Leakage Through the Clearance Between Piston and Cylinder in Hermetic Compressors. *Purdue University, Purdue e-Pubs*

[21] MC Allister, 2016, RL natural response, Khan Academy

[22] Alkan Göcmen et al, 2016, ‘An engine layout study for common rail systems in large diesel engines’, CIMAC 2016-094, 03 Fuel Injection & Gas Admission

[23] Shin endo, Yuseke Adachi, Yoshiki Ihara et al. ‘Development of J-series Engine and Adoption of Common Rail Fuel Injection System’. *SAE Transactions* Vol. 106, Section 3: JOURNAL OF ENGINES (1997), pp. 1096-1109

Nomenclature

VARIABLES

A	Sectional Area	[m^2]
b	Damping Coefficient	[-]
C_d	Discharge Coefficient	[-]
$clrc$	Length of the Clearance	[mm]
D	Diameter	[mm]
E	Electric Potential	[V]
F	Force	[N]
g	Gravitational Acceleration	[m/s^2]
H	Lift	[mm]
I	Current	[A]
K	Spring Coefficient	[-]
K_f	Bulk Modulus of Fuel	[Pa]
L	Length	[mm]
L	Electrical Inductance	[H]
m	Mass	[kg]
n	Rotational Speed	[rpm]
P	Fuel Pressure	[bar]
$\dot{Q}$	Volumetric Flowrate	[m^3/s]
q	Volumetric Flowrate	[m^3/s]
R	Electrical Resistance	[Ω]
$RACK$	Fuel Rack Setting	[-]
r	Radius	[m]
t	Time	[s]
V	Volume	[m^3]
$\dot{V}$	Volumetric Change	[m^3/s]
v	Velocity	[m/s]
x	Displacement	[m]
$\dot{x}$	Velocity	[m/s]
$\ddot{x}$	Acceleration	[m/s^2]

Greek Letters

α	Cam Angle	[degree]
α_B	Half Wrapping Angle of the Cam	[degree]
β	Area Ratio	[-]
ε	Eccentricity of the Cam	[-]
θ	Circular Angle	[degree]
μ	Flow Coefficient	[-]
ξ	Opening of the Inlet Port	[-]
ρ	Density	[kg/m^3]
ϕ	Angle	[degree]

Subscripts

ac	Accumulation Chamber
$blck$	Blocked Area
brl	Barrel
c	Cam
cyl	Cylinder
d	Damping Force
e	Engine
dv	Delivery Valve
hlx	Helix
hyd	Hydraulic Force
ic	Injection Chamber
in	Inlet
inj	Injection
$leak$	Leakage
mag	Magnetic Force
$n; N$	Needle Valve

orf	Orifice
out	Outlet
P	Plunger Pump
pc	Pressure Control Chamber
r	Resistance Force *(the Mechanical Injection Model)*
r	Common Rail *(the Common-Rail Injection Model)*
s	Spring Force
$spill$	The Spilling Phase of Pump
$supply$	The Supplying Phase of Pump
t	Tank
$tank$	Flowrate from the Tank
$ublck$	Unblocked Area
V	The Ball Valve

Appendix: List of The Pre-Set Constants

This thesis is carried out with limited data, the constants in the model, unless is mentioned in the thesis that was measured from the real engine, are all manually set. Although the constants and geometric parameters are chosen based on previous literature and within the reasonable scale, further researches that based on the models are still highly recommended to justify the pre-set constants . In addition, the injection models provided by this thesis can be customized to simulate different type of injection systems by changing the pre-set data:

Table 18. The Pre-Set Data

	Name	*Variable name as in the model*	*Pre-set Value*	*[Unit]*
Cam Model	Rotating speed	*n_e*	1	[Hz]
	Start of injection	*inj_start*	0	[degree]
	Rise angle of the cam	*phi_r*	60	[degree]
	Dwell angle of the cam	*phi_d*	0	[degree]
	Fall angle of the cam	*phi_f*	60	[degree]
	Maximum lift	*H_c*	0.025	[m]
Inlet Port	Height of the inlet port	*H_orf*	$0.2 \cdot H\_c$	[m]
	Length of the helix	*L_hlx*	0.00523	[−]
	Radius of the inlet port	*r_i*	1e-3	[m]
Pump Model	Length of the Clearance	*clrc*	0.0001	[m]
	Fuel return pressure	*P_t*	10	[bar]
	Barrel height	*L_p*	0.27	[m]
	Plunger Diameter	*D_p*	0.017	[m]
	Radius of the delivery orifice	*r_dv*	2.64e-3	[m]
	Maximum lift of delivery valve	*H_dvmax*	0.01	[m]
	Diameter of flowback orifice	*D_fb*	0.015	[m]
Mechanical Injector	Needle Area (bigger end)	*A_n*	2.4674e-04	[m^2]
	Needle Area (smaller end)	*A_s*	8.2247e-05	[m^2]
	Needle Mass	*m_n (in the Simulink block)*	1.3	[kg]
	Area of Injection Holes	*'Nozzle Hole Area' (in the Simulink block)*	(4.5e-4^2)*1/4*pi	
	Injector Volume	*V_s0*	0.0000002	[m^3]

	Name	*Variable name as in the model*	*Pre-set Value*	*[Unit]*
Solenoid Model	Inductance	*L*	0.01	[H]
	Electrical Resistance	*R*	5	[Ω]
	Starting Voltage	*V_st*	60	[V]
	Maintaining Voltage	V_{mt}	40	[V]
	Start of Activation	*t_start*	0	[s]
The Ball Valve	Magnetic Force	*F_mag (in the Simulink block)*	40 · I	[N]
	Area of the valve's ball	A_v	2.2760e-05	[m^2]
	Maximum Lift of the Ball Valve	Ha_max	0.015	[m]
	Mass of the Ball Valve	m_a	0.2	[kg]
The Needle Valve and The Injection Chamber	Rail Pressure	P_rail	200	[bar]
	Area of the servo piston	A_pis	4.9348e-04	[m^2]
	Maximum Lift of the Needle	Hn_max	0.004	[m]
	Area of the Injector Inlet port	*(to adjust in the Simulink block)*	(1e-3^2)*1/4*pi	[m^2]
	Area of the nozzle hole	*(to adjust in the Simulink block)*	(5.5e-4^2)*1/4*pi	[m^2]
	Initial Volume of the injection chamber	*(to adjust in the Simulink block)*	0.000001	[[m^3]]

Besides the constants listed above, the setting of spring constants and damping coefficients can also be improved if more accurate data is available.